

Comparative Molecular Dynamics Simulation Studies of Realistic Eukaryotic, Prokaryotic, and Archaeal Membranes

Irina D. Pogozheva,[⊥] Grant A. Armstrong,[⊥] Lingyang Kong,[⊥] Timothy J. Hartnagel,[⊥] Carly A. Carpino, Stephen E. Gee, Danielle M. Picarello, Amanda S. Rubin, Jumin Lee, Soohyung Park, Andrei L. Lomize, and Wonpil Im*



Cite This: *J. Chem. Inf. Model.* 2022, 62, 1036–1051



Read Online

ACCESS |



Metrics & More

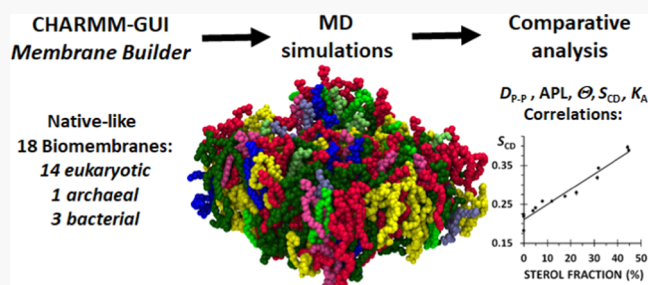


Article Recommendations



Supporting Information

ABSTRACT: We present a comparative all-atom molecular dynamics simulation study of 18 biomembrane systems with lipid compositions corresponding to eukaryotic, bacterial, and archaeobacterial membranes together with three single-component lipid bilayers. A total of 105 lipid types used in this study include diverse sterols and glycerol-based lipids with acyl chains of various lengths, unsaturation degrees, and branched or cyclic moieties. Our comparative analysis provides deeper insight into the influences of sterols and lipid unsaturation on the structural and mechanical properties of these biomembranes, including water permeation into the membrane hydrocarbon core. For sterol-containing membranes, sterol fraction is correlated with the membrane thickness, the area compressibility modulus, and lipid order but anticorrelated with the area per lipid and sterol tilt angles. Similarly, for all 18 biomembranes, lipid order is correlated with the membrane thickness and area compressibility modulus. Sterols and lipid unsaturation produce opposite effects on membrane thickness, but only sterols influence water permeation into the membrane. All membrane systems are accessible for public use in CHARMM-GUI Archive. They can be used as templates to expedite future modeling of realistic cell membranes with transmembrane and peripheral membrane proteins to study their structure, dynamics, molecular interactions, and function in a native-like membrane environment.



1. INTRODUCTION

The biological membranes are the frontier between the internal and the external cell environments and separate intracellular compartments. They are highly complex systems containing lipids, hydrophobic molecules, and proteins that either span the membrane or are permanently or transiently inserted into one side. Membrane-spanning proteins represent ~25% of protein-coding genes in all organisms (e.g., ~5000 transmembrane proteins in human) and are responsible for all vital cellular functions, including cell recognition, signal transduction, molecular and ion transport, energy production, and anabolic and catabolic metabolism.¹ Biogenesis, self-organization, and functional activity of membrane proteins are controlled and modulated by the lipid composition.² Therefore, interplay between proteins and lipids defines cell shape, organelle morphology, and membrane physical and mechanical properties that regulate all processes in membranes.^{3–5}

A typical cell membrane contains hundreds of lipid types that are asymmetrically distributed between two leaflets and also differ in lipid head groups and in the length and degree of saturation of their acyl chains.⁶ Simple organisms, such as bacteria, have a lipidome characterized by a limited diversity of head groups but highly variable acyl chains, including branched lipids (with iso- and anteiso-fatty acids)⁷ or lipid containing

cyclic groups (e.g., cyclopropane).⁸ In Gram-negative bacteria, the lipid variability is primarily associated with lipopolysaccharides (LPS) from the outer membranes (OM), which are composed of lipid A with typically six acyl chains, core oligosaccharide, and O-antigen polysaccharide.^{9,10} In contrast to bacterial and eukaryotic membranes formed by glycerol-based lipids (GLs) (having *sn*-glycerol-3-phosphate backbone, ester linkages, and fatty acid chains attached to the *sn*-1 and *sn*-2 positions), archaeobacterial membranes are characterized by *sn*-glycerol-1-phosphate backbone, ether linkages, and isoprenoid acyl chains containing 20, 25, or 40 carbon atoms.¹¹ All archaeal halophiles and some methanogens have lipids based on archaeol (2,3-di-phytyl-*sn*-glycerol) with the glycerol moiety linked to different polar head groups.¹¹

Eukaryotic membranes are mainly composed of glycerol-based lipids (GLs), sphingolipids (SLs), and sterols.^{12–14} The lipid types and fatty acid profiles significantly vary in different

Received: December 15, 2021

Published: February 15, 2022



eukaryotic cells and intracellular organelles.¹⁵ To ensure such a great lipid diversity, eukaryotic organisms use ~5% of their genes.¹² The eukaryotic membranes are mainly composed of phosphatidylcholine (PC) and phosphatidylethanolamine (PE) and, to a less extent, of phosphatidylserine (PS), phosphatidylglycerol (PG), phosphatidic acid (PA), cardiolipin (CL), diacylglycerol (DAG), sphingolipid-based glycolipids, and diverse phosphatidylinositols (PI). The common GLs of eukaryotic and bacterial membranes are PE, PG, and CL lipids. Thylakoid membranes of plants and photosynthetic bacteria are enriched in glycerol-based glycolipids, such as neutral monogalactosyldiacylglycerol (MGDG), digalactosyldiacylglycerol (DGDG), and negatively charged sulfoquinovosyldiacylglycerol (SQDG).¹⁶ Among GLs, CL, abundant in mitochondrial inner membranes, is negatively charged (-1 or $-2e$) with a unique structure of four acyl chains attached to two PA moieties that are connected by glycerol. Due to its cone shape that can induce a negative curvature, CL plays an important role in regulating the organization and function of mitochondrial proteins, as well as fission and fusion of mitochondrial membranes.¹⁷ Bis(monoacylglycerol)phosphate (BMP), an exclusive glycerophospholipid (PL) of late endosomes and lysosomes, has two acyl chains on the *sn*-2 position of two glycerol backbones linked together by PA, which can move to the *sn*-3 position by acyl migration.¹⁸ The negatively charged and cone-shaped BMP plays important roles in membrane binding and activation of enzymes for membrane digestion and in promoting membrane invaginations during the formation of multivesicular bodies.¹⁸

SLs have a sphingosine backbone, 16–24 carbon acyl chain attached to the amine group, and head groups that are composed of a hydroxyl group (in ceramide), PC (in sphingomyelin), or highly diverse carbohydrates (in gangliosides). The most common lipid acyl chains of GLs and SLs include palmitic acid (16:0), oleic acid (18:1), stearic acid (18:0), linoleic acid (18:2), palmitoleic acid (16:1), myristic acid (14:0), arachidonic acid (20:4), and docosahexaenoic acid (22:6).¹³ Membranes of plants and algae are enriched in linoleic acid (18:2) and linolenic acid (18:3).¹⁹

Sterols have a hydrophobic four-fused ring core, a short acyl tail, and hydrophilic groups attached to the C3 atom of the core. In mammals, the most common sterol is cholesterol (CHOL), which is primarily located in plasma membranes (PMs), reaching up to 10–50 mol % of their lipid content.²⁰ CHOL affects physicochemical properties of membranes,^{21,22} induces the formation of liquid-ordered (Lo) phase and lipid segregation into nanoscale domains,¹³ and decreases membrane permeability.²³ Plants have a large variety of phytosterols, among which the most common ones are sitosterol, campesterol, and stigmasterol.²⁴ In many fungi, including baker's yeast, ergosterol represents a dominant sterol.²⁵

PC, PG, PS, SL, PI, DGDG, and SQDG are cylindrically shaped lipids that spontaneously assemble into bilayer (lamellar) structures, while PE, PA, MGDG, DAG, BMP, CL, and CHOL are cone-shaped lipids that are preferable for nonbilayer structures with a negative curvature, such as an inverted hexagonal phase or a cubic phase.²⁶ Cone-shaped lipids along with curvature-promoting membrane proteins are key factors regulating the membrane curvature.⁵ Incorporation of nonbilayer lipids into membranes imposes curvature stress that affects membrane protein structure, function, and

oligomerization and promotes membrane fusion, fission, and budding.^{26,27}

Despite considerable efforts in experimental studies of membrane proteins and the great progress in structure determination techniques, our understanding of molecular interactions between proteins and lipids in their native membranes is still limited. Computational modeling and simulation of cell membranes give an opportunity to analyze protein behaviors in their natural membrane environment. It has been demonstrated that using realistic membrane complexity is essential for reproducing the energetics of conformational transitions in membrane proteins.²⁸

During the last 35 years, molecular simulations of lipid membranes have substantially evolved from studies of single-component bilayers²⁹ to modeling realistic cellular membranes with various lipid types.³⁰ The progress became rapid with the development of accurate force fields, programs to simulate membrane models, and tools to preassemble lipids in a bilayer.^{31–33} Recent advancements in computing technology have made it routine to perform all-atom molecular dynamics (MD) simulations on the time scale of hundreds of nanoseconds, enabling proper equilibration of membrane bilayers, and, in some cases, simulations lasting tens of microseconds.^{30,34}

Historically, MD simulations have focused on increasing the complexity of individual biological membranes by expanding lipid diversity³⁵ and by implementing membrane asymmetry.³⁶ This required developments of tools for easy building of membranes with complex lipid compositions^{31,32} and improvements to computational approaches.³⁷ For example, all-atom MD simulations of membranes with natively like lipid composition have been performed for the outer^{38–41} and inner membranes of Gram-negative bacteria,^{42–45} cell membrane of Gram-positive bacteria,⁴⁶ archaeobacterial membranes,⁴⁷ PM and organelle membranes of yeast,^{48–50} and PM of plants,^{28,51} among others. These membrane systems usually included up to 600 lipids of 4–10 lipid types that were simulated on the nano- to microsecond (ns– μ s) time scale. The larger multicomponent membrane systems that require long simulations for proper sampling are less practical using all-atom force fields but can be modeled at the coarse-grained (CG) resolution.⁵² Recently, CG simulations (up to 10 μ s) using Martini lipid models were applied to characterize thylakoid membranes of plants (2044 lipids of 7 types) and cyanobacteria (2044 lipids of 5 types).⁵³ Rather long (~ 80 μ s) GC simulations have been performed for the idealized “average” mammalian PM composed of ~ 20 000 lipids of 63 types⁵⁴ and for the “brain-like” PM of a similar size.^{52,55}

Comparison of computational results with experimental data supports the reliability of MD simulations.⁵⁶ When experimental and simulation data are in good agreement, computational approaches provide more detailed interpretations of experimental data on atomic, molecular, and macroscopic (material) levels. Results of MD simulations describe general properties of biomembranes, including their mechanical (bending rigidity, compressibility, fluidity, etc.), structural (thickness, tilt angles, area per lipid, lipid tail order parameters, mass density profiles, and location of molecules within the bilayer), and physicochemical properties (polarity profiles, lateral heterogeneity, transition from Lo to liquid-disordered (Ld) phase, and formation of nanoscale lipid domains).⁵⁷

In this study, we have performed all-atom MD simulations of 18 biomembrane systems with natively like lipid compositions

Table 1. Lipid Compositions of 18 Biomembranes

system	leaflet	head group	molar ratio	acyl chains	sterol %	unsat. % ^a	#double bond/tail	ref
PMm	inner	PC:PE:PI:PS:PA:SM:CHOL	(18:26:5:11:1:10:29)	16:0, 18:0, 18:1, 18:2, 20:4, 24:1	29.0	53.5	1.1	54
	outer	PC:PE:SM:CMH:CHOL	(38:6:22:4:37)		34.6	57.9	0.8	
PMf	inner	PC:PE:PI:PS:PA:ERG	(16:21:20:31:8:4)	16:0, 16:1, 18:1	4.0	65.6	0.7	48
	outer	PC:PE:PI:PS:PA:ERG:MIPC	(11:7:5:7:3:49:54)		36.0	59.8	0.6	
PMp	inner	PC:PE:PA:PI:PS:PG:DG:DG:STEROL	(20:24:11:5:2:4:2:32)	16:0, 18:1, 18:2, 18:3	32.0	51.5	1.2	19
	outer	PC:PE:PA:PS:CMH:STEROL	(13:16:5:1:15:64)		56.1	55.0	1.1	
ERm	both	PC:PE:PI:PS:SM:PA:CHOL	(61:20:6:3:4:1:5)	16:0, 18:0, 18:1, 18:2, 20:4	5.0	47.2	1.2	60
ERf	both	PC:PE:PI:PS:PA:ERG	(47:14:23:8:4:4)	16:0, 16:1, 18:1	4.0	83.9	0.8	48
GOLm	both	PC:PE:PI:PS:SM:LPC16:CHOL	(45:17:9:4:12:5:8)	16:0, 18:0, 18:1, 18:2, 20:4, 22:0	8.0	36.3	0.9	60
GOLf	both	PC:PE:PI:PS:PA:ERG	(34:11:37:3:3:12)	16:0, 16:1, 18:1	12.0	73.9	0.7	48
ENDm	both	PC:PE:PI:SM:CHOL	(33:13:8:16:32)	16:0, 18:0, 18:2, 20:4, 22:6, 24:0	31.4	50.0	1.7	61
LYSm	both	PC:PE:PI:PS:SM:CHOL:BMP	(35:2:5:8:3:6:18:7)	16:0, 18:0, 18:1, 18:2, 20:4, 22:6, 24:0	17.6	54.2	1.7	62, 63
MOM	inner	PC:PE:PI:PS:PA	(54:20:22:3:1)	16:0, 18:0, 18:1, 18:2, 20:4	0	50.0	1.6	64, 65
	outer	PC:PE:PI:PS:PA:CL	(54:38:4:1:1:2)		0	52.0	1.6	
MIM	inner	PC:PE:PI:PS:CL	(29:36:6:3:26)	16:0, 18:0, 18:1, 18:2, 20:4	0	70.6	1.8	64, 65
	outer	PC:PE:PI:PS:CL	(58:37:5:3:11)		0	58.8	1.6	
VAC	both	PC:PE:PI:PS:PG:CMH:DG:MG:DG:SQ:DG:STEROL	(14:21:7:1:1:13:3:2:2:5:1)	12:0, 16:0, 18:1, 18:2, 18:3	44.3	36.3	0.7	66
THYp	both	PG:DG:DG:MG:DG:SQ:DG	(15:30:40:15)	16:0, 16:1, 18:3	0	85.0	2.4	53
THYb	both	PG:DG:DG:MG:DG:SQ:DG	(9:24:43:24)	16:0, 18:1	0	42.9	0.4	53
aPM	both	PG:CL:AROL:MEN-8	(64:7:8:21)	C20, C25	0	10.9	0.9	67
G-OM	inner	PE:PG:CL	(75:20:5)	16:0, 16:1, 18:1	0	50.0	0.5	38, 39
	outer	LPS (1)		C12, C14	0	0.0	0	
G-IM	both	PE:PG:CL	(79:19:2)	15:0, 16:0, 16:1, 18:1, cy17:0	0	26.0	0.2	42
G+PM	both	PG:PE:CL	(65:27:8)	C14:0, aC15:0, iC15:0, C16:0	0	0.0	0	44, 68

^aFraction of lipids with double bonds in acyl tails.

corresponding to 14 eukaryotic cellular and organelle membranes, the outer and the inner membranes of Gram-negative bacteria (*Escherichia coli*), and cell membranes of Gram-positive bacteria and archaeobacteria. A comparative analysis of structural and mechanical parameters obtained from these simulations allows us to describe the properties of diverse biological membranes and to obtain deeper insight into the effects of sterols and lipid unsaturation on membrane properties, including water permeation into the membrane hydrocarbon core.

2. METHODS

2.1. Eighteen Biomembrane Systems. To analyze the influence of lipid diversity on biological membrane properties, we chose 18 model systems with complex lipid compositions: plasma membranes of mammals (PMm), plants (PMp), and fungi (PMf), endoplasmic reticulum (ER) membranes of mammals (ERm) and fungi (ERf), apparatus Golgi membranes of mammals (GOLm) and fungi (GOLf), mammalian membranes of endosomes (ENDm) and lysosomes (LYSm), mitochondrial outer (MOM) and inner membranes (MIM), plant vacuole membranes (VAC), thylakoid membranes of plants (THYp) and cyanobacteria (THYb), archaeobacterial plasma membranes (aPM), outer (G-OM) and inner (G-IM) membranes of Gram-negative bacteria, and plasma membranes of Gram-positive bacteria (G+PM) (Table 1). For each system, we selected the most abundant lipid types with various head groups and acyl chains based on experimental studies of different membranes and using compositions of the previously simulated mammalian, plant, yeast, and bacterial membranes (see the Supporting Information, Tables S1–S18). Overall, we used 105 lipid types, including diverse sterols and glycerol-based lipids with acyl chains of various lengths, unsaturation degree, and with branched or cyclic moieties. To compare properties of complex and simple membranes, we also built three homogeneous systems composed of 1,2-dioleoyl-*sn*-glycero-3-phosphocholine (DOPC), 1-palmitoyl-2-oleoyl-*sn*-glycero-3-phosphocholine (POPC), and 1,2-dipalmitoyl-*sn*-glycero-3-phosphocholine (DPPC).

2.2. Addition of New Lipids to CHARMM-GUI Membrane Builder. A total of 59 lipids (underlined ones in Tables S1–S18) were newly constructed and added to the Membrane Builder^{58,59} lipid library for this study. These include palmitoylated sterols, glycosylated sterols, new variants of PG lipids present in the thylakoid plant system, and other PLs.

2.3. System Setup and MD Simulation Protocol. A summary of chosen lipids and their number in each system is shown in Tables 1 and S1–S18. On average, each system comprises ~100 lipids per leaflet. All systems in this study are particularly noteworthy for their complexity, in some cases containing up to 23 different lipid types. PMm, PMf, PMp, G-OM, MOM, and MIM were built asymmetrically, while all other membranes were built symmetrically. For the asymmetric membrane systems, following the suggested procedure,³⁷ the symmetric bilayer system of each leaflet's components was first built and equilibrated. Then, an asymmetric membrane system was built by adjusting the number of lipids in each leaflet to match the membrane area of each leaflet.

All systems were generated by Membrane Builder,^{58,59} and all simulations were performed using OpenMM⁶⁹ with inputs generated by CHARMM-GUI.⁷⁰ Table S19 shows the initial

system sizes and the numbers of water and ions (e.g., 150 mM NaCl). Ca²⁺ ions were added for G-OM to neutralize the negative charges in the LPS lipid A and inner core parts. Following Membrane Builder's default six-step equilibration protocol,^{33,49} the NVT (constant particle number, volume, and temperature) dynamics was first applied with a 1 femtosecond (fs) time step for 250 picoseconds (ps). Subsequently, the NPT (constant particle number, pressure, and temperature) ensemble was applied with a 1 fs time step (for 125 ps) and with a 2 fs time step (for 1.5 ns). During the equilibration, positional and dihedral restraint potentials were applied to carbohydrate, lipid, and water molecules, and their force constants were gradually reduced. A production run was performed for 1 μ s for each system (i.e., three replicas per membrane type) with a 4 fs time step using the hydrogen mass repartitioning technique^{71,72} without any restraint potential. The SHAKE algorithm was applied to the bonds containing hydrogen atoms.⁷³ The van der Waals interactions were cutoff at 12 Å with a force-switching function between 10 and 12 Å,⁷⁴ and electrostatic interactions were calculated by the particle-mesh Ewald method.⁷⁵ The temperature (assigned differently for different systems above the gel-to-liquid crystal phase transition in Table S19) and the pressure (at 1 bar) were controlled by Langevin dynamics with a friction coefficient of 1 ps⁻¹ and a semi-isotropic Monte Carlo barostat, respectively.^{76,77}

2.4. Simulation Analysis. Trajectories were analyzed for the following membrane properties: the membrane area (i.e., XY system area), the membrane thickness ($D_{p,p}$), the area compressibility modulus (K_A), the deuterium order parameters (S_{CD}), the sterol tilt angle (Θ), the mass density profiles (MDPs), and the area per lipid (APL). Quantitative assessment of membrane properties is reported as an average and standard error of three replicas over the last 500 ns of each simulation unless otherwise stated. This was done to ensure that each system had proper time to equilibrate.

2.4.1. XY Membrane Area. The membrane area was monitored as a function of time to check the simulation equilibration. The XY dimensions changed in accordance with one another throughout the simulation (i.e., $X = Y$), so only changes to the X dimension were reported. As shown in Figure S1, all systems were well equilibrated during the first 500 ns.

2.4.2. Thickness ($D_{p,p}$). The $D_{p,p}$ was measured as the distance between the average Z positions of all phosphate groups in the inner and outer leaflets (close to the distance between lipid head groups, D_{HH} ⁷⁸). In addition, we evaluated the hydrophobic thickness ($2D_C$) and the distance between lipid carbonyls (D_{CG}) (Table S20). $2D_C$ was calculated as the distance between the average Z positions of the first aliphatic carbons of each acyl chain in each leaflet. D_{CG} was calculated as the distance between the average Z positions of carbonyl carbons in each leaflet or ether oxygens for lipids with no carbonyl carbons.

2.4.3. Area Compressibility Modulus (K_A). The K_A characterizing the membrane area compressibility (i.e., the resistance of a bilayer to isotropic area expansion or compression) was calculated by $K_A = k_B T \langle A \rangle / \langle \delta A^2 \rangle$, where k_B is the Boltzmann constant, T is the temperature, $\langle A \rangle$ is the average system area, and $\langle \delta A^2 \rangle$ is the mean square fluctuation of A. For each system, the final 500 ns trajectory was split into two blocks in three replicas to calculate the average and standard error of K_A .

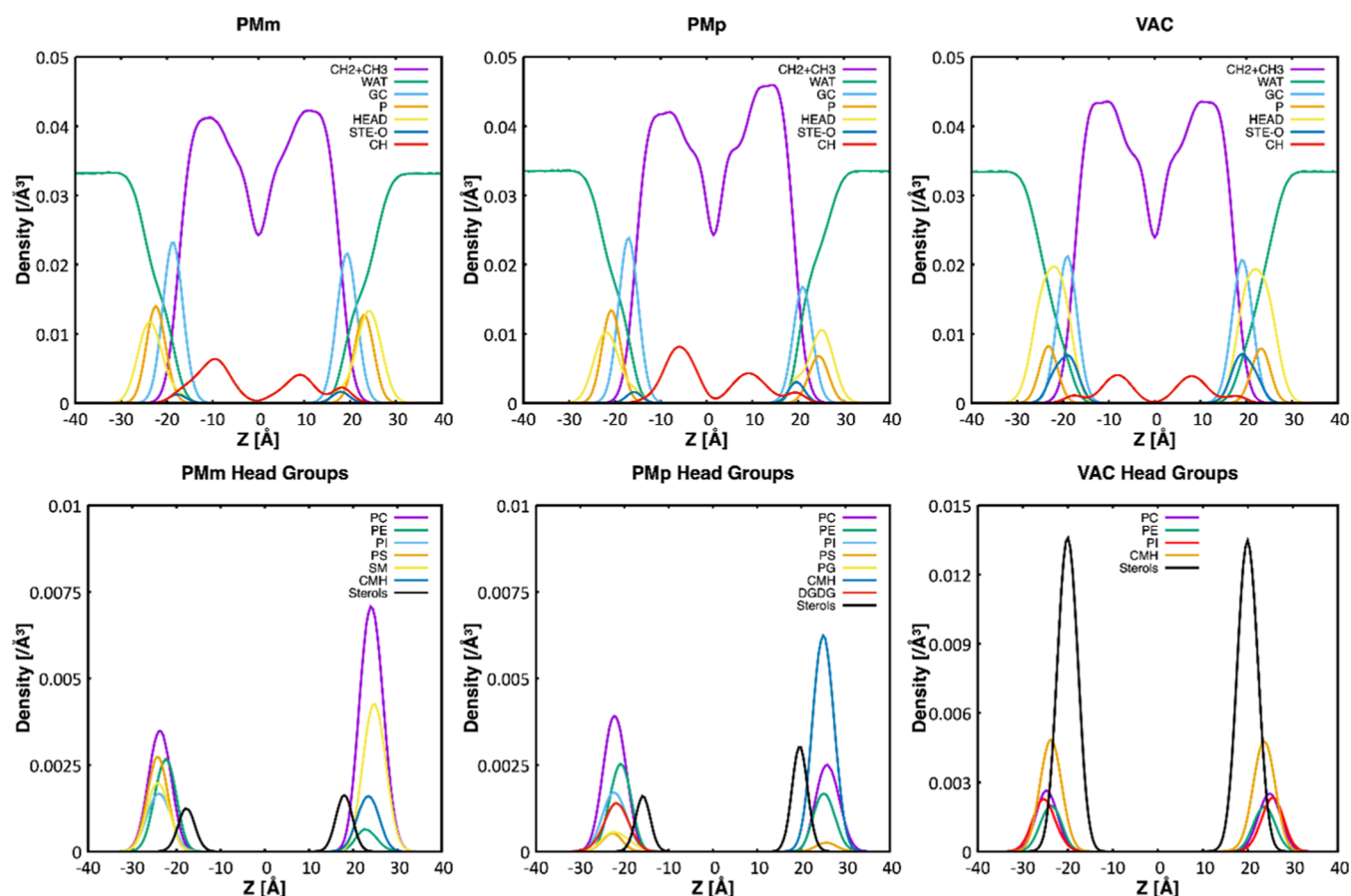


Figure 1. Mass density profiles (MDPs) of PMm, PMp, and VAC. Note that the membrane is centered at $Z = 0$, and the outer leaflet corresponds to $Z > 0$.

2.4.4. Deuterium Order Parameters (S_{CD}). The S_{CD} characterizing the acyl chain order (i.e., bilayer fluidity) was calculated by $S_{CD} = \langle 3 \cos^2 \theta - 1 \rangle / 2$, where θ is the angle between the C–H vector and the bilayer membrane normal (i.e., the Z -axis). Due to different lipid compositions, it is not realistic to generalize S_{CD} for all acyl chains. Instead, the calculated S_{CD} is based on the 16:0 *sn*-1 chain of the most abundant lipid in each system, since the 16:0 *sn*-1 chain is present in almost all systems. For aPM, the calculated S_{CD} is based on C20 *sn*-1 chain.

2.4.5. Sterol Tilt Angle (Θ). The Θ was calculated as an angle between the vector of sterols (from C17 to C3) and the Z -axis. The sterols include CHOL, β -sitosterol, stigmasterol, ergosterol, campesterol, and their derivatives, depending on the system.

2.4.6. Mass Density Profiles (MDPs). The Z -dependent system component MDPs were calculated for lipid acyl tails ($\text{CH}_2 + \text{CH}_3$), double-bonded acyl tails (CH), carbonyl and glycerol groups (GC), phosphate groups (P), head groups (HEAD), sterol oxygens (STE-O), and water (WAT). Each MDP was calculated as an average of three replicas with a bin size of 0.5 Å for $-40 < Z < 40$ Å. Note that the membrane is centered at $Z = 0$, and the outer leaflet corresponds to $Z > 0$.

2.4.7. Water Penetration Depths (D_{H_2O}). Based on water MDPs, the D_{H_2O} in both leaflets were calculated as the distances (from $Z = 0$) showing less than 1% of bulk water density.

2.4.8. Area Per Lipid (APL). Since most systems are heterogeneous, Voronoi tessellation was used to determine the APL of each lipid type using the following atom selections: C21, C31, and C2 for PLs (see POPC in Table S1), C2S, C3S, and C1F for SLs (see SSM in Table S1), and O3 for sterols (see CHOL in Table S1). All results are given in Tables S1–S18. In addition, the average APL of each system was calculated by dividing the membrane area by the total number of lipids in each leaflet.

3. RESULTS AND DISCUSSION

3.1. Simulation of Mammalian, Yeast, and Fungi Plasma Membranes. Lipid compositions of eukaryotic PMs are highly complex, asymmetric, and dynamic, and the relative amounts of lipids vary in different cell types.¹² Here, we simulated three PM systems: mammals (PMm), plants (PMp), and fungi (PMf) containing 11, 18, and 9 lipid types, respectively (Tables S1–S3).

PMm contains the most abundant lipid types from the average human PM.⁵⁴ PMp represents membranes of mung bean hypocotyl¹⁹ that have a more complex lipid mixture than previously modeled plant PMs containing up to 10 lipid types.^{28,51} The lipid composition of PMf is similar to that of the previously modeled yeast PM,⁴⁸ although half of sterol molecules is substituted by an inositol-containing SL, mannosyl-inositol-phosphoryl-ceramide (MIPC) based on the work of Hechtberger et al.⁷⁹

The lipid distribution in all three PM systems is asymmetric and similar to experimental data in that the majority of SLs are

Table 2. Comparison of the Calculated Membrane Properties in This Study with Data from Published MD Simulations of Similar Biological Membranes^a

membrane	D_{p-p} (Å)	APL (Å ²) (out/in)	Θ (deg)	S_{CD} (out/in)	K_A (dyn/cm)	D_{H_2O} (Å) (in/out) ^d	reference
PMm	45.5	45.5/48.7	14.1	0.34	633	-14.2/14.7	this study
average PM	41	51/55	N/A	0.43/0.36	N/A	N/A	54
PMf	42.2	43.3/58.9	13.3	0.28	877	-8.3/17.6	this study
PM1	43.4	47.4	17.9	0.35	570	-12.0/12.0	48
PMp	45.3	41.6/47.4	11.3	0.39	1306	-12.7/16.5	this study
Top10	42.0	42.9/45.7	N/A	N/A	N/A	N/A	28
soybean root	42.7 ^b	52.7	18	0.25	510	-12.0/12.0	51
soybean hypocotyl		51.9		0.30	570		
ERm	40.2	62.2	22.3	0.24	264	-11.0/11.0	this study
ERf	37.9	63.0	24.1	0.23	358	-10.0/10.0	this study
ER1	37.8 ^b	64.0	27.3	0.23	290	-10.0/10.0	48
GOLm	41.9	57.1	20.6	0.26	289	-11.6/11.6	this study
GOLf	39.6	54.5	21.7	0.26	384	-11.0/11.0	this study
TGN1	38.6 ^b	60.6	26.3	0.22	280	-10.0/10.0	48
ENDm	44.9	49.6	16.1	0.32	452	-14.0/14.0	this study
LYSm	42.2	56.6	19.7	0.27	368	-12.3/12.3	this study
VAC	46.3	46.8	11.4	0.40	1510	-15/14.8	this study
MOM	39.5	66.2/66.2	N/A	0.22	265	-10.3/10.9	this study
MIM	39.1	73.8/78.1	N/A	0.23	293	-10.9/10.5	this study
THYp	39.0	65.4	N/A	0.22	313	-9.8/9.8	this study
plant membrane 293 K	28.0 ^c	66.0	N/A	N/A	311	-12.0/12.0	53
THYb	41.1	63.0	N/A	0.22	211	-10.6/10.6	this study
cyanobacterial membrane 293 K	30.0 ^c	64.0	N/A	N/A	350	N/A	53
aPM	43.3	69.7	N/A	0.15	187	-9.5/10.2	this study
20-MK8	37.8 ^c	N/A	N/A	0.16	268	-10.0/10.0	47
DPhPC, 298 K	37.0 ^b	76.1	N/A	0.18	605	N/A	44
G-OM	36.6	182.3/63.8	N/A	0.23	1573	-9.2/10.0	this study
LPS-PL	24.7 ^c	180	N/A	0.24	N/A	-10.0/9.0	39
G-IM	38.3	64.0	N/A	0.23	417	-10.3/10.3	this study
TOP6	37.3 ^b	64.0	N/A	0.23	340	-10.0/10.0	42
G+PM	37.0	61.5	N/A	0.22	289	-9.2/9.2	this study
SaCM	~40	61.8	N/A	N/A	N/A	-10.0/10.0	46
DOPC	38.8	67.5	N/A	0.18	308	-10.0/10.0	this study
DOPC, 303 K	38.0 ^b	67.4	N/A	0.18 ^e	265 ^f	-10.0/10.0	81, 82d 83,e
DPPC	39.7	61.5	N/A	0.22	220	-9.3/9.3	this study
DPPC, 323 K	38.0 ^b	63.1	N/A	N/A	N/A	-10.0/10.0	81
POPC	39.0	64.4	N/A	0.22	325	-9.6/9.6	this study
POPC, 303 K	37.0 ^b	68.3	N/A	N/A	N/A	-10.0/10.0	84

^aFor clarity, only the average values are reported in this table. ^b D_{HH} , the distance between lipid head groups. ^c $2D_C$, the hydrophobic thickness; Table S20 summarizes the calculated $2D_C$ values in this work. ^d D_{H_2O} , water penetration depths, when reported from the literature, were approximated from the MDP figures of the relevant systems; negative values correspond to the inner leaflet; and positive values correspond to the outer leaflet. N/A, not available.

in the outer leaflets, and 80% of PE, PA, PI, and almost all PS are in the cytosolic leaflet.⁸⁰ Importantly, these three PM systems significantly differ in the content and distribution of PC lipids, SLs, and sterols (Figure S2). PC lipids account for 27% of lipids in PMm with their 70% located in the outer leaflet, while in PMf and PMp, PE lipids are the major PL, while PC lipids account for less than 15% of lipids and their 60% is located in the inner leaflet. Sterols and SLs comprise almost half of all lipids in all PMs, but a sterol:SL ratio significantly differs among systems (e.g., 2:1 in PMm, 1:1 in PMf, and 6:1 in PMp). Thus, PMm has 32% of CHOL and 17% of SLs; PMp is characterized by the high content (45%) of diverse phytosterols, while PMf contains almost equal amounts (~25%) of ergosterol and MIPC. Although the percent of unsaturated lipids is slightly higher in PMf (~63 vs ~56% in PMm and ~53% in PMp), the number of double

bonds per tail is higher in PMp (1.15 vs 0.95 in PMm and 0.65 in PMf) due to the abundance of 18:2 and 18:3 acyl chains in PMp (Table 1 and Figure S3).

The mass density profiles (MDPs) for aliphatic lipid groups are more asymmetric in PMp and PMf than in PMm, possibly due to the substantial sterol asymmetry (Figures 1, S4, and S5). In the MDPs of all PMs, there is one maximum for double bonds (CH) in the inner leaflet ($Z < 0$) but two such maxima in the outer leaflet that correspond to cis-double bonds of PLs and trans-double bonds of SLs, respectively. The PMp MDPs show a significant increase of CH maxima relative to those in PMm and PMf due to their higher fraction of polyunsaturated acyl chains. Water profiles indicate that in all asymmetric PM systems, water penetrates much deeper into the membrane hydrophobic core from the inner side (up to $Z = -14.2$ Å for PMm, -12.7 Å for PMp, and -8.3 Å for PMf) than from the

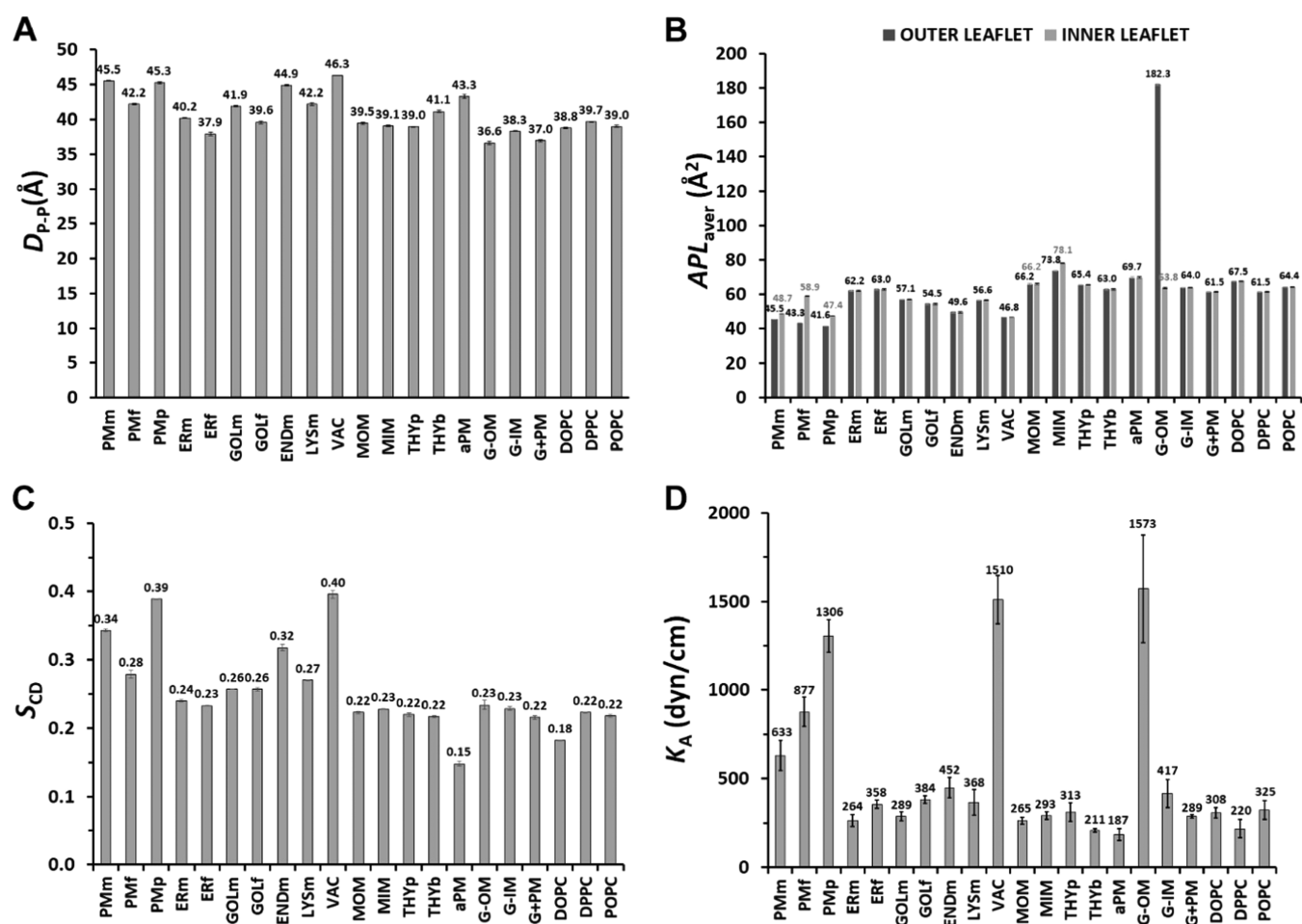


Figure 2. Various membrane properties calculated in this work. (A) Membrane thickness ($D_{p,p}$). (B) Average area per lipid (APL). The black bars are for the outer leaflet and the gray bars are for the inner leaflet; the symmetric membrane has the same bars. (C) Order parameters (S_{CD}). (D) Area compressibility modulus (K_A). Calculation details are given in the [Methods](#) section.

outer side (up to $Z = 14.7$ Å for PMm, 16.5 Å for PMp, and 17.6 Å for PMf). This result indicates that the PM outer leaflets containing more sterols are more ordered and less water permeable than the inner leaflets. The difference is especially pronounced in the case of PMf, which has a sterol ratio of 4:36 between the inner and the outer leaflets. As shown in [Table 2](#), the average APL from the PMf inner leaflet is larger than in the outer leaflet by 15.6 Å², which further supports this observation.

Despite variances in lipid composition, the membrane properties of three PMs ($D_{p,p}$, average APL, S_{CD} , and K_A) are not dramatically different ([Table 2](#) and [Figure 2](#)). The high order of acyl chains (characterized by S_{CD} larger than 0.28) is a likely cause of the upright orientation of sterol rings in PMs (average tilt angle of $\sim 13^\circ$) ([Figure 3A,B](#)). The previously obtained membrane properties of the average human PM,⁵⁴ yeast PM,⁴⁸ and the soybean root and hypocotyl PMs⁵¹ are close to our data for the corresponding PM systems ([Table 2](#)).

3.2. Modeling of Eukaryotic Organelle Membranes.

3.2.1. Endoplasmic Reticulum. Membranes of endoplasmic reticulum (ER) have a nearly symmetric lipid distribution between both leaflets that are mainly composed of PC, PE, and PI lipids with a minor fraction of other lipid types.¹² In this study, we simulated ER membrane systems of mammals (ERm) and fungi (ERf) with 12 and 9 lipid types, respectively ([Tables S4](#) and [S5](#)). The lipid composition of ERm

corresponds to that of rat liver microsomes,⁶⁰ while the lipid content in our ERf system is similar to that in the previously modeled yeast ER membranes.⁴⁸ Both ERm and ERf have symmetric lipid distributions in both leaflets with a PC:PE:PI ratio of 61:20:6 and 47:14:23, respectively. Interestingly, although ERm has a much lower fraction of unsaturated lipids (47% in ERm vs 84% in ERf), it has more double bonds per lipid tail (1.2 vs 0.8 in ERf) ([Table 1](#)) due to the presence of polyunsaturated fatty acids (18:2, 20:4) in ERm and only monounsaturated acyl tails in ERf ([Figure S3](#)).

Our simulations show that the membrane properties of both ER systems are quite similar but significantly different from those of the three PM systems ([Figures 2](#) and [3](#)). The MDPs show that ERf membranes are slightly thinner (by 2.3 Å) than ERm, but water penetration depths (D_{H_2O}) are quite similar for both membranes (up to $Z = \pm 10$ Å for ERf and ± 11 Å for ERm) ([Table 2](#) and [Figure S4](#)). Comparison of ER and PM systems reveals higher average APL and sterol tilt angles and lower $D_{p,p}$, S_{CD} , and K_A for ER membranes, indicating that ER membranes are more disordered than PMs. Looser lipid packing in the ER bilayer could facilitate insertion of newly synthesized lipid and protein molecules into ER membranes, as well as the formation and budding out of vesicles and lipid droplets.

3.2.2. Golgi Apparatus. Golgi apparatus is made of stacks of vesicular cisternae with tubular connections that participate in

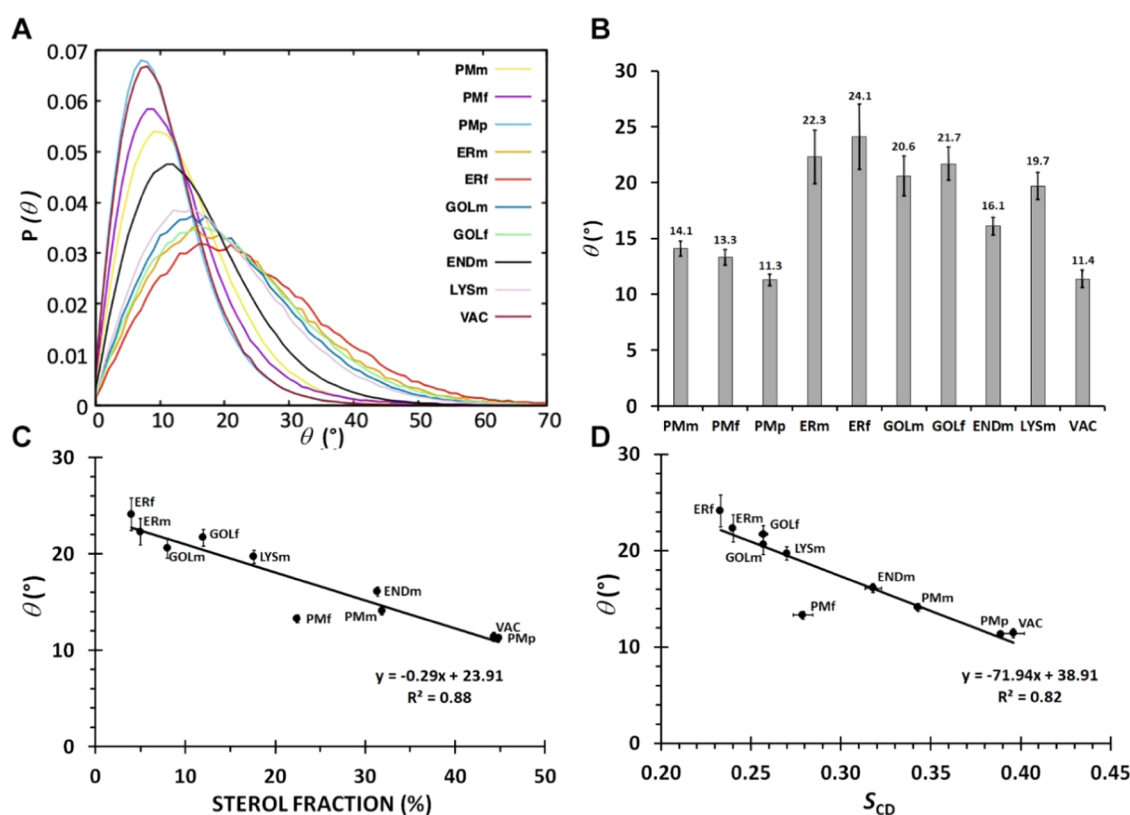


Figure 3. (A) Distributions of sterol tilt angles and (B) their average values in 10 eukaryotic membrane systems containing sterols. (C) Sterol tilt angle vs sterol fraction. (D) Sterol tilt angle vs order parameters (S_{CD}).

vesicular transport in the secretory, lysosomal, and endocytic pathways. Although trans-Golgi network (TGN) is known to have an asymmetric lipid distribution between leaflets, we simulated two symmetric membrane systems of Golgi apparatus from mammals (GOLm) and fungi (GOLf) containing 13 and 10 lipid types, respectively (Tables S6 and S7). The lipid composition of GOLm corresponds to that in rat liver Golgi membranes,⁶⁰ while the lipid composition of GOLf is similar to that in the previously modeled yeast TGN1 system.⁴⁸ The most evident differences between lipid contents of GOLm and GOLf are in PI lipids (9% in GOLm vs 37% in GOLf) and SLs (12% in GOLm and absent in GOLf).

The membrane properties of GOLm and GOLf (Table 2; Figures 2 and 3) are rather similar, including D_{H_2O} (up to $Z = \pm 11$ Å for GOLf and ± 11.6 Å for GOLm) (Figure S4). As shown in Table 2, our calculations show slightly smaller average APL and sterol tilt angles and higher values of D_{p-p} , S_{CD} , and K_A for GOLf than the corresponding values obtained in the previous yeast TGN1 simulations in which the simulation time was only 200 ns with a different van der Waals interaction switching method.⁴⁸ Therefore, our GOLf system appears to be a bit more rigid and ordered than in the previous simulation.

3.2.3. Endosomes and Lysosomes. The lipid composition of early endosomes resembles that of PMs. However, membranes of late endosomes and lysosomes differ from PMs by an increasing amount of acidic lipids and a high level (up to 70%) of BMP, a poorly degradable nonbilayer phospholipid.¹⁸ Our membrane models of mammalian endosomes (ENDm) and lysosomes (LYSm) contain 11 and 13 lipid types, respectively (Tables S8 and S9). The lipid composition of ENDm⁶¹ is similar to that of PMm (Table

1). LYSm contains anionic lipids, PI, PS, and BMP (8, 3, and 7 mol %, respectively), in addition to PC, PE, SL, and CHOL, the major lipid types of PMm and ENDm.^{62,63} The degree of acyl chain unsaturation in both systems is similar to that in PMm, but the number of double bonds per lipid tail is higher (Table 1).

As expected, the membrane properties of ENDm resemble those of PMm (Table 2; Figures 2 and 3). LYSm has slightly lower D_{p-p} , S_{CD} , K_A , and higher average APL and cholesterol tilt angle, compared to ENDm and PMm. These data indicate more disordered LYSm, which is probably due to the significant presence of anionic and nonbilayer lipids. This observation is further supported by the MDPs that show deeper water penetration into the hydrophobic region of LYSm (up to $Z = \pm 12.3$ Å) than those of ENDm (up to $Z = \pm 14$ Å) and PMm (up to $Z = -14.2$ and $+14.7$ Å) (Figure S4).

3.2.4. Outer and Inner Mitochondrial Membranes. In this study, we modeled asymmetric mitochondrial outer (MOM) and inner (MIM) membranes containing 10 and 9 lipid types, respectively (Tables S10 and S11). The MOM system is mainly composed of PC, PE, and PI lipids (54, 29, and 13 mol %, respectively), while MIM has PC, PE, and CL lipids as major phospholipids (41, 34, and 17 mol %, respectively).^{64,65} As shown in Table 1, both MIM and MOM have a large number of double bonds (1.6–1.8 double bonds per lipid tail), though MIM has more unsaturated lipids than MOM (70.6% in the inner leaflet and 58.8% in the outer leaflet) due to the abundance of eicosatetraenoic (20:4) and linoleic (18:2) fatty acids in MIM. Despite some differences in the lipid content, the membrane properties of MOM and MIM are almost identical (Table 2 and Figure 2). The MDPs also show similar

distributions of lipid components and deep $D_{\text{H}_2\text{O}}$ (up to $Z = \pm 10.5 \text{ \AA}$) in both MOM and MIM (Figure S4).

3.2.5. Vacuoles. Vacuoles are the largest organelles in plant cells. They participate in the transport and storage of ions and metabolites and in cell turgor. Our vacuole membrane (VAC) system contains 23 lipid types that are symmetrically distributed between leaflets. It was modeled based on the lipid composition of the tonoplast membrane from *Acer pseudoplatanus* cells.⁶⁶ VAC is composed of phospholipids (39 mol %), glycolipids (18 mol %), sterols (13 mol %), and glycosylated sterols (31 mol %) (Table S12) and is characterized by a high content of palmitic (16:0) and linoleic (18:2) acyl chains that account for 54 and 23% of all fatty acids. The predominant phospholipid is PE (50% more than PC). This lipid composition is similar to that of PMp, though two-thirds of sterols are glycosylated in VAC (Table 1). The membrane properties of VAC are close to those of PMp (Table 2; Figures 2 and 3), but the symmetric MDPs of lipid components and water penetration profiles for VAC (up to $Z = \sim \pm 15 \text{ \AA}$) resemble those of PMm (Figure 1).

3.2.6. Thylakoid Membranes. Thylakoid membranes form compartments inside chloroplasts and their postulated ancestors, cyanobacteria. This is the site of all light-dependent processes of photosynthesis, i.e., the conversion of light energy into chemical energy. The characteristic features of photosynthetic membranes in plants and cyanobacteria are unusual abundance of nonphosphorus galactoglycerolipids, underrepresentation of phospholipids, and presence of anionic sulfolipids.^{16,85} Lipids of thylakoid membranes include a sole phospholipid, PG, and three glycolipids (MGDG, DGDG, and SQDG).

We simulated thylakoid membranes of plants (THYp) and cyanobacteria (THYb) containing seven and five lipid types, respectively (Tables S13 and S14). The lipid compositions of these systems are similar to those modeled previously.⁵³ Both systems contain four lipid classes (PG, DGDG, MGDG, and SQDG) at a ratio of 15:30:40:15 (THYp) and 9:24:43:24 (THYb). The major difference is the level of lipid unsaturation, which is increased in THYp (Table 1). Accordingly, the intensity of double bond (CH) peaks in the MDPs is greater in THYp than in THYb (Figure S4).

Both systems have similar structural parameters ($D_{\text{P-P}}$, average APL, and S_{CD}) (Table 2 and Figure 2), as well as $D_{\text{H}_2\text{O}}$ (up to $Z = \pm 9.8 \text{ \AA}$ for THYp and $\pm 10.6 \text{ \AA}$ for THYb) (Figure S4). The increased K_{A} of THYp (313 ± 54 vs 211 ± 9 dyn/cm for THYb) may indicate slightly more rigid membranes of plants. This is different from the CG simulation results, where the photosynthetic membranes of cyanobacteria were more rigid.⁵³ According to our results, both THYb and THYp have relatively high fluidity and low lipid order, which are similar to those of mitochondrial membranes (Table 2 and Figure 2).

3.3. Simulation of Archaeobacterial Membranes with Menaquinone-8. The archaeobacterial membranes are formed by isopranyl glycerol ether lipids, such as 1,2-diphytanoyl-*sn*-glycero-3-PC (DPhPC), which is an important factor for adaptation to extreme temperatures, acidity, and salinity. Haloarchaea are one of the largest groups of archaea that can thrive in high salt environments and withstand temperatures up to $50 \text{ }^\circ\text{C}$, a wide pH range (from 4 to 10), and extreme levels of oxidative stress. Membranes of haloarchaea are highly unsaturated, mainly due to the presence of menaquinones (MENs) that reach up to 72% of the total lipids.⁶⁷ MENs with

1,4 naphthoquinine head group function as electron/proton carriers in the photosynthetic cycle,⁸⁶ while their polyunsaturated isoprenoid tails supposedly play an antioxidative role as scavengers of free radicals.⁸⁷

Our model of archaeobacterial plasma membranes (aPM) was built from more common acidic, neutral archaeal lipids, and menaquinone-8 (MEN-8) at a ratio of 71:8:21⁶⁷ (Table S15). This lipid composition differs from the previous MD simulation systems of archaeal membranes that were composed of acidic (PG-AR) and zwitterionic (PE-AR) isoprenoid GLs at 3:2 and with increasing MEN-8 concentration from 0 to 50 mol %.⁴⁷

Despite the different lipid compositions, the current aPM model reproduces the main structural features of the previously simulated membrane system with 20 mol % of MEN-8 (20-MK8). In particular, the MDPs of aPM (Figures S4 and S5) show an increased membrane thickness ($D_{\text{P-P}} = 43.3 \text{ \AA}$) due to the accumulation of the major fraction of MEN-8 at the membrane midplane, as in the previous study of 20-MK8.⁴⁷ At the same time, the distribution of MEN-8 head groups along the Z -axis is rather broad (Figure S5), indicating that some of them are located at the membrane/water interface, while their isoprenoid chains are aligned along the membrane normal and intercalate with lipid acyl chains. In addition, S_{CD} for C20 acyl chains has three plateaus (Figure S6), which is consistent with other simulations of bilayers with diphytanoyl lipids.^{44,47}

aPM has the lowest K_{A} and S_{CD} , and a rather deep water penetration profile (up to $Z = -9.5 \text{ \AA}$ and $+10.2 \text{ \AA}$), indicating that aPM is less ordered than any other biomembrane systems in this study (Table 2 and Figure 2). The K_{A} for the pure DPhPC bilayer is higher ($K_{\text{A}} = 605$ dyn/cm at 298 K)⁴⁴ than in aPM ($K_{\text{A}} = 187$ dyn/cm). In addition, aPM is thinner and more loosely packed than 20-MK8⁴⁷ (Table 2). It is possible that acidic lipids and a low level of MEN-8 significantly perturb not only the hydrophobic core but also the head group packing at the membrane/water interface, resulting in the more distorted and disordered bilayer with a reduced water-barrier function.

3.4. Simulation of Bacterial Membranes.
3.4.1. Outer Membrane of Gram-Negative Bacteria. Unlike a typical phospholipid bilayer, the Gram-negative bacterial outer membrane (OM) has an extremely asymmetric structure, where the inner leaflet is composed of PLs, primarily PE, PG, and CL lipids, and the outer leaflet contains unique lipopolysaccharides (LPS).^{88,89} We have previously simulated LPS-containing OMs of *E. coli* and other Gram-negative bacteria.^{38–41} In this study, we generated an outer membrane of the Gram-negative bacteria (G-OM) system that has the same lipid composition of the asymmetric LPS-PL system of *E. coli*³⁹ (Table S16): 35 molecules of lipid A-R1 core in the outer leaflet and PE, PG, and CL lipids at a ratio of 75:20:5 in the inner leaflet. The membrane properties of G-OM were almost identical to those found previously (Table 2).

In comparison with other biomembrane systems, as shown in Table 2, G-OM has a decreased membrane thickness ($D_{\text{P-P}}$ of 36.6 \AA) and the highest value of K_{A} . These results show that due to the presence of LPS and their electrostatic crosslinking via divalent ions (Ca^{2+}), G-OM is much stiffer than all other biomembranes considered in this study. The APL in the outer leaflet is 182.3 \AA^2 or approximately 30 \AA^2 per acyl chain, which is close to the experimental value of 26 \AA^2 .⁹⁰

3.4.2. Inner Membrane of Gram-Negative Bacteria. The inner membrane of Gram-negative bacteria (G-IM) is less

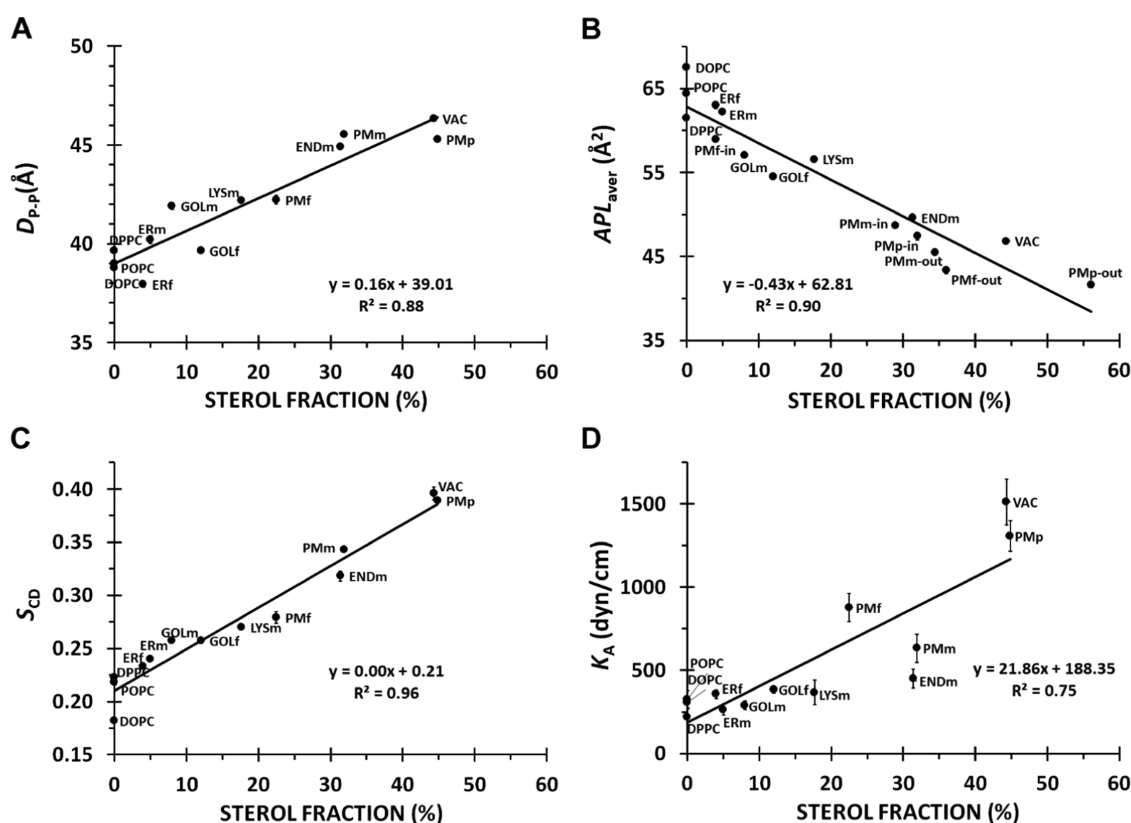


Figure 4. Correlation of sterol fraction in sterol-containing 10 membrane systems with (A) membrane thickness (D_{p-p}), (B) average area per lipid (APL), (C) order parameters (S_{CD}), and (D) compressibility modulus (K_A). For asymmetric PMm, PMp, and PMf, the average APLs in the inner and the outer leaflets are shown separately. Three single-component lipid bilayers devoid of sterols are also included for comparison.

complex than PMs of eukaryotic cells. However, as an adaptation to environmental conditions, bacteria often develop modifications of their acyl tails, such as the incorporation of cyclic moieties. It has been shown that the inclusion of the cyclopropane ring decreases the surface density of the bilayer and produces a more rigid membrane compared to membranes with no cyclopropane ring in acyl chains.⁴²

We generated a G-IM system composed of seven lipid types with PE:PG:CL at a ratio of 79:19:2 that contain cyclopropane rings in their *sn*-2 acyl tails (Table S17). This lipid composition is close to that of the previously modeled TOP6 system,⁴² except the added 2 mol % of CL. Consequently, the membrane properties of G-IM are almost identical to those of TOP6 (Table 2), except for a slightly higher value of K_A (417 dyn/cm in G-IM vs 340 dyn/cm in TOP6). Overall, the properties of G-IM are similar to those of mitochondrial and thylakoid membranes (Figure 2).

3.4.3. Plasma Membrane of Gram-Positive Bacteria. Lipid composition of Gram-positive bacterial plasma membranes (G+PM) is variable and depends on the environmental conditions.⁹¹ Mechanisms of bacteria adaptation to a wide range of temperature include regulation of the lipid fatty acid iso/anteiso composition⁹¹ or the unsaturation level.⁹² We modeled G+PM based on the lipid composition of *Bacillus subtilis* (a Gram-positive bacterium) that contains PE (27 mol %), PG (65 mol %), and CL lipids (8 mol %) (Table S18). Most lipid tails are branched due to the presence of iso/anteiso C15 fatty acids in both *sn*-1 and *sn*-2 positions (Figures S2 and S3).

Lipid membranes with iso/anteiso C15 fatty acids have been previously modeled for *Chlamydia trachomatis*⁴⁴ (a Gram-

negative bacterium) and *Staphylococcus aureus* (a Gram-positive bacterium).⁴⁶ However, their lipid compositions were quite different from our G+PM system; in the former case, model bilayers contained PC lipids with branched fatty acids, while the latter system contained 57 mol % PG, 5 mol % CL, and 38 mol % of a positively charged lysylphosphatidylglycerol (Lys-PG). It has been shown that acyl tail branching increases average APL, K_A , and lipid axial relaxation times in the corresponding lipid bilayers relative to the DPPC bilayer while decreasing lipid chain order and changing MDPs.⁴⁴ However, our G+PM system shows only a slight increase of the average APL and K_A relative to DPPC, while the S_{CD} and MDPs of G+PM and DPPC are very similar (Figures 2, S4, and S5).

3.5. Comparative Analysis of 18 Biomembrane Systems. MD simulations of 18 biomembrane systems with distinct lipid compositions provide us a unique opportunity to make a comparative analysis of membrane properties of all of these different biological membranes. From our simulations, PMm, PMp, PMf, and VAC have the highest membrane rigidity, tighter lipid packing, and greater acyl chain order, especially in their outer leaflets, than all other membranes. This conclusion is based on the lowest APL and the largest K_A , D_{p-p} , and S_{CD} for PMs and VAC (Table 2; Figures 2 and 3). Overall, the membrane rigidity and lipid order decrease in the following sequence: PMs and VAC > ENDm and LYS > GOLm and GOLf > ERM and ERf, which is based on the decreasing D_{p-p} , S_{CD} , and K_A , as well as the increasing average APL and cholesterol tilt angles. A similar trend was found previously for the membranes of yeast organelles.⁴⁸

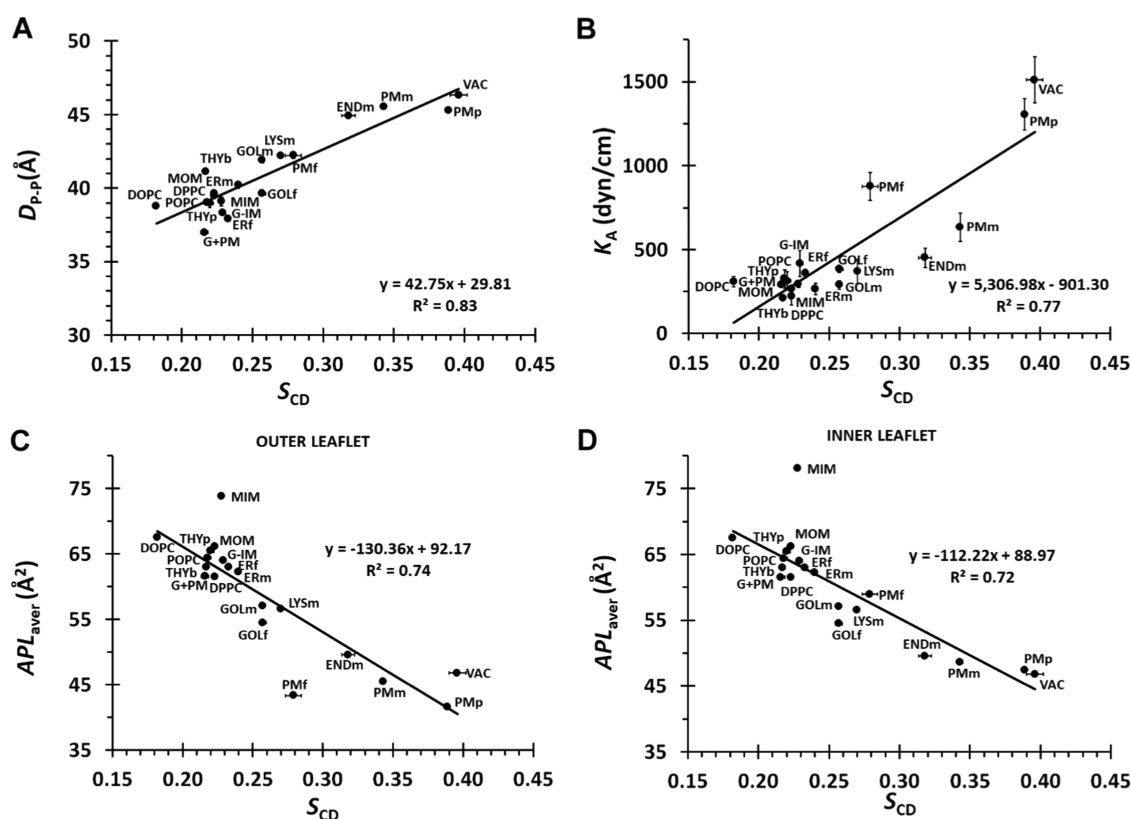


Figure 5. Correlation of acyl chain order (S_{CD}) in 16 multicomponent and 3 single-component membrane systems with (A) membrane thickness (D_{P-P}), (B) area compressibility modulus (K_A), (C) average area per lipid (APL) in the outer leaflet, and (D) average APL in the inner leaflet. Note that aPM and G-OM systems are excluded from all scatter plots as outliers.

Interestingly, despite largely different lipid compositions, mitochondrial membranes (MOM and MIM), thylakoid membranes (THYb and THYp), and bacterial cell membranes (G-IM and G+PM) are characterized by much lower rigidity and lipid order, which distinguishes them from PMs, VAC, and ENDm. Two notable outliers are the LPS-containing G-OM and aPM. In G-OM, acyl chain packing is tighter than those in artificial bilayers composed of typical membrane lipids (DOPC, DPPC, POPC), although still less dense than PMs, ENDm, and VAC (Figure 2). This compact packing could be critical to ensure the protective properties of the bacterial OM as a permeability barrier. Our aPM system, which is mainly formed by phytanyl-ether acidic lipids with 20 mol % of MEN-8, shows the lowest K_A and S_{CD} among all systems considered in this study. Such low stiffness and high fluidity probably arise from the broad distribution MEN-8 along the membrane normal, causing membrane thickening and disordering.

A more detailed comparative analysis of 18 biomembrane systems allows us to uncover the role of sterols and lipid unsaturation in the structural and mechanical properties of these biological membranes and their effects on membrane permeability to water, which is elaborated below.

3.5.1. Role of Sterols and Lipid Order. It is well documented that CHOL affects the physicochemical properties of membranes, such as mechanical strength, area per lipid, lipid order, and thickness,²¹ induces the formation of Lo phase and lipid segregation into nanoscale domains,¹³ and decreases membrane permeability.²³

In this study, 10 of 18 systems contain various levels of sterols, and sterol levels are different in the inner and the outer leaflets of PMm, PMp, and PMf. To investigate the influence of

sterols on the membrane properties, we analyzed the dependencies of structural and mechanical parameters on sterol fraction in these 10 systems that represent different eukaryotic cellular and organelle membranes. For comparison, pure DOPC, POPC, and DPPC lipid bilayer lacking sterols are also considered. As shown in Figure 4, sterol fraction shows strong correlations with D_{P-P} (correlation coefficient, R^2 of 0.88), average APL (R^2 of 0.90), S_{CD} (R^2 of 0.96), and K_A (R^2 of 0.75), indicating that the fraction of sterols in a membrane plays a key role in the lipid order (S_{CD}), membrane thickness (D_{P-P}), lipid packaging (characterized by the average APL), and, in a lesser extent, the membrane stiffness and ability to resist dilation and compression (characterized by K_A).

In membranes with higher sterol content and lipid order (S_{CD}), sterol molecules align more vertically with respect to the membrane normal, and thus their average tilt angles decrease (Figure 3C,D). Clearly, sterols increase membrane thickness, lipid order parameter, area compressibility modulus, and decrease area per lipid in eukaryotic cellular and organelle membranes. Our findings for biological membranes with complex lipid mixtures are in line with previous results of computational^{21,93} or experimental⁹⁴ studies of simpler cholesterol-containing lipid bilayers.

Since sterols produce the main effect on the lipid order, we analyzed how the membrane properties of biological membranes lacking sterols depend on S_{CD} . This analysis can be applied to all 18 complex biomembrane systems and three artificial lipid bilayers. As shown in Figure 5, there is a good correlation between membrane thickness and S_{CD} (R^2 of 0.82), though slightly worse correlations are observed between S_{CD} and K_A (R^2 of 0.77) and between S_{CD} and the average APL (R^2

of 0.74 (outer leaflet) and 0.72 (inner leaflet)). The notable outlier in the latter case is the MIM system, which contains 17 mol % CL (10% in the outer leaflet and 26% in the inner leaflet) with a high APL value (APL \sim 134 \AA^2 for CL vs APL \sim 63 \AA^2 for POPC, see Table S11).

3.5.2. Role of Lipid Unsaturation. All eukaryotic cellular and organelle membranes studied here are characterized by a high degree of lipid unsaturation. More than 35% of their lipids have at least one double bond in their acyl chains, although many lipids contain polyunsaturated chains (e.g., 18:2, 18:3, 20:4, 22:6) (Table 1). To analyze the effect of lipid unsaturation on the membrane properties while excluding the effect of sterols, we selected eukaryotic membranes lacking sterols (MOM, MIM, THYp, and THYb) and analyzed their leaflets separately. As shown in Figure 6A, there is a modest

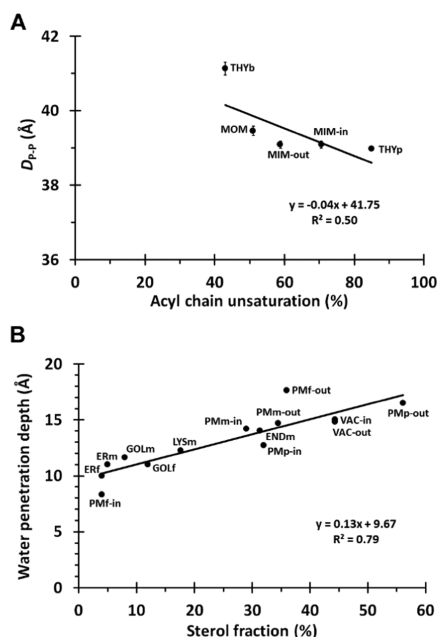


Figure 6. Correlation of acyl chain unsaturation in sterol-free eukaryotic membranes with membrane thickness ($D_{p,p}$) (A). Correlation of water penetration depth as the distance from the membrane center ($Z = 0$ is the membrane center) with sterol fraction in sterol-containing membranes (B). Data for the inner and the outer leaflets of asymmetric systems are included separately as both leaflets have different degrees of acyl unsaturation or sterol fraction.

correlation between the acyl chain unsaturation level and $D_{p,p}$ (R^2 of 0.50). However, there is no significant correlation between the acyl chain unsaturation level and the average APL, K_A , or S_{CD} for these membrane systems (data not shown). These results indicate that higher lipid unsaturation slightly reduces the membrane thickness. A similar tendency was experimentally observed for SOPC ($D_{p,p} = 40.7$ \AA) and DOPC ($D_{p,p} = 36.9$ \AA).⁸³ Thus, the presence of sterols and lipid unsaturation produce opposite effects on the membrane thickness.

3.5.3. Water Penetration Depths. To understand the ability of water to penetrate into the hydrophobic core of various biological membranes, we analyzed water MDPs of all 18 membrane systems (Figure S4) and obtained the D_{H_2O} for each leaflet. As shown in Figure 6B, D_{H_2O} significantly increases in eukaryotic membranes with a higher sterol fraction (R^2 of 0.79). However, there is no significant effect of acyl chain

unsaturation on D_{H_2O} in sterol-free MOM, MIM, THYp, and THYb (data not shown). Apparently, sterols are more important than lipid double bonds for creating additional permeability barriers below lipid carbonyl regions that prevent water from entering into the membrane hydrophobic core. This conclusion complies with experimental observations of CHOL reducing the membrane penetration of water⁹⁵ and the bilayer permeability.⁹⁴

4. CONCLUSIONS

In this work, we present all-atom MD simulations of 18 biomembrane systems with complex lipid mixtures corresponding to diverse eukaryotic, bacterial, and archaeobacterial membranes. Lipid bilayer systems are composed of 4–23 lipid types, including diverse sterols, glycerol-based lipids, and sphingolipids with acyl tails of various lengths, degree of saturation, and branched and cyclic moieties. In addition, Membrane Builder in CHARMM-GUI⁹⁶ has been expanded to cover 59 new lipid types for this study and used to build all biomembrane systems composed of 200–250 lipids for the symmetric or asymmetric bilayer systems.

Modeling and simulation of different nativelike membranes allow us to characterize and to compare their structural and mechanical properties, including mass density profiles of lipid components and water molecules, localizations and tilt of sterols in the lipid bilayer, bilayer thicknesses, lipid tail order parameters, areas per lipid, and area compressibility moduli. The comparative analysis provides deeper insight into the role of sterols and lipid unsaturation on the membrane properties, including water penetration depths into the hydrophobic core of various biomembranes. Our analysis shows that sterols increase membrane thickness, ordering, and stiffness and prevent water penetration into the membrane hydrophobic core. Unlike sterols, the increased lipid unsaturation slightly decreases the membrane thickness but does not significantly affect other membrane properties.

All simulated membrane systems are accessible for public use in CHARMM-GUI Archive (<https://www.charmm-gui.org/docs/archive/biomembrane>). They can be used as templates to expedite future modeling of realistic cell membranes with transmembrane and peripheral membrane proteins to study their structure, dynamics, molecular interactions, and function in a nativelike membrane environment.

■ ASSOCIATED CONTENT

Supporting Information

The Supporting Information is available free of charge at <https://pubs.acs.org/doi/10.1021/acs.jcim.1c01514>.

Lipid compositions and area per lipids of 18 biomembranes (Tables S1–S18); initial system size, simulation temperature, and numbers of water and ions for each biomembrane system (Table S19); hydrophobic thickness ($2D_C$), membrane thickness between phosphate groups ($D_{p,p}$), and membrane thickness between carbonyl groups (D_{CC}) for each biomembrane system (Table S20); time series of the X dimension of each biomembrane system (Figure S1); lipid type distribution in each biomembrane system (Figure S2); lipid acyl chain distribution in each biomembrane system (Figure S3); mass density profiles in 18 biomembrane systems (Figure S4); head group density

profiles in 18 biomembrane systems (Figure S5); and deuterium order parameters of *sn*-1 16:0 acyl chain in 18 biomembrane systems (Figure S6) (PDF)

AUTHOR INFORMATION

Corresponding Author

Wonpil Im – Department of Biological Sciences, Lehigh University, Bethlehem, Pennsylvania 18015, United States; Department of Bioengineering and Department of Chemistry, Lehigh University, Bethlehem, Pennsylvania 18015, United States; orcid.org/0000-0001-5642-6041; Email: wonpil@lehigh.edu

Authors

Irina D. Pogozeva – Department of Medicinal Chemistry, College of Pharmacy, University of Michigan, Ann Arbor, Michigan 48109, United States; orcid.org/0000-0002-3024-9574

Grant A. Armstrong – Department of Biological Sciences, Lehigh University, Bethlehem, Pennsylvania 18015, United States; orcid.org/0000-0003-4016-6841

Lingyang Kong – Department of Bioengineering, Lehigh University, Bethlehem, Pennsylvania 18015, United States; orcid.org/0000-0002-5020-1527

Timothy J. Hartnagel – Department of Chemistry, Lehigh University, Bethlehem, Pennsylvania 18015, United States; orcid.org/0000-0001-7958-398X

Carly A. Carpino – Department of Bioengineering, Lehigh University, Bethlehem, Pennsylvania 18015, United States; orcid.org/0000-0003-3338-5421

Stephen E. Gee – Department of Bioengineering, Lehigh University, Bethlehem, Pennsylvania 18015, United States; orcid.org/0000-0001-7934-4196

Danielle M. Picarello – Department of Biological Sciences, Lehigh University, Bethlehem, Pennsylvania 18015, United States; orcid.org/0000-0001-5270-3259

Amanda S. Rubin – Department of Bioengineering, Lehigh University, Bethlehem, Pennsylvania 18015, United States; orcid.org/0000-0001-9087-5342

Jumin Lee – Department of Biological Sciences, Lehigh University, Bethlehem, Pennsylvania 18015, United States; orcid.org/0000-0002-1008-0118

Soohyung Park – Department of Biological Sciences, Lehigh University, Bethlehem, Pennsylvania 18015, United States; orcid.org/0000-0002-4883-3031

Andrei L. Lomize – Department of Medicinal Chemistry, College of Pharmacy, University of Michigan, Ann Arbor, Michigan 48109, United States; orcid.org/0000-0002-3044-7597

Complete contact information is available at: <https://pubs.acs.org/10.1021/acs.jcim.1c01514>

Author Contributions

[†]I.D.P., G.A.A., L.K., and T.J.H. contributed equally to this work.

Notes

The authors declare no competing financial interest. All simulated membrane systems are available in the CHARMM-GUI Archive (<https://www.charmm-gui.org/docs/archive/biomembrane>).

ACKNOWLEDGMENTS

The authors thank Sang-Jun Park for creating the CHARMM-GUI Archive page. This work was part of the Data4Impact summer undergraduate program at Lehigh University and was supported in part by grants from NSF MCB-1810695 (WI), DBI-2011234 (WI), DBI-2010851 (AL and IP).

ABBREVIATIONS

aPM, archaeobacterial plasma membranes; G+PM, plasma membranes of Gram-positive bacteria; G-IM, inner membranes of Gram-negative bacteria; G-OM, outer membranes of Gram-negative bacteria; ENDM, mammalian membranes of endosomes; ERf, endoplasmic reticulum membranes of fungi; ERm, endoplasmic reticulum membranes of mammals; GOLf, apparatus Golgi membranes of fungi; GOLm, apparatus Golgi membranes of mammals; LYSm, mammalian membranes of lysosomes; MIM, mitochondrial inner membranes; MOM, mitochondrial outer membranes; PMf, plasma membranes of fungi; PMm, plasma membranes of mammals; PMp, plasma membranes of plants; THYb, thylakoid membranes of cyanobacteria; THYp, thylakoid membranes of plants; VAC, plant vacuole membranes; BMP, bis(monoacylglycerol)-phosphate; CHOL, cholesterol; CL, cardiolipin; DAG, diacylglycerol; DGDG, digalactosyl-diacylglycerol; DOPC, 1,2-dioleoyl-*sn*-glycero-3-phosphocholine; DPhPC, 1,2-diphytanoyl-*sn*-glycero-3-PC; DPPC, 1,2-dipalmitoyl-*sn*-glycero-3-phosphocholine; GLs, glycerol-based lipids; LPS, lipopolysaccharide; MEN, menaquinone; MGDG, monogalactosyl-diacylglycerol; PA, phosphatidic acid; PC, phosphatidylcholine; PE, phosphatidylethanolamine; PG, phosphatidylglycerol; PI, phosphatidylinositol; PL, phospholipid; POPC, 1-palmitoyl-2-oleoyl-*sn*-glycero-3-phosphocholine; PS, phosphatidylserine; SL, sphingolipid; SQDG, sulfoquinovosyl-diacylglycerol; APL, area per lipid; CG, coarse grained; MDPs, mass density profiles; MD, molecular dynamics

REFERENCES

- (1) Von Heijne, G. The Membrane Protein Universe: What's out There and Why Bother? *J. Intern. Med.* **2007**, *261*, 543–557.
- (2) Corradi, V.; Sejdiu, B. I.; Mesa-Gallosa, H.; Abdizadeh, H.; Noskov, S. Y.; Marrink, S. J.; Tieleman, D. P. Emerging Diversity in Lipid-Protein Interactions. *Chem. Rev.* **2019**, *119*, 5775–5848.
- (3) Nyholm, T. K. Lipid-Protein Interplay and Lateral Organization in Biomembranes. *Chem. Phys. Lipids* **2015**, *189*, 48–55.
- (4) Corradi, V.; Sejdiu, B. I.; Mesa-Gallosa, H.; Abdizadeh, H.; Noskov, S. Y.; Marrink, S. J.; Tieleman, D. P. Emerging Diversity in Lipid-Protein Interactions. *Chem. Rev.* **2019**, *119*, 5775–5848.
- (5) Jarsch, I. K.; Daste, F.; Gallop, J. L. Membrane Curvature in Cell Biology: An Integration of Molecular Mechanisms. *J. Cell Biol.* **2016**, *214*, 375–387.
- (6) Sud, M.; Fahy, E.; Cotter, D.; Brown, A.; Dennis, E. A.; Glass, C. K.; Merrill, A. H., Jr; Murphy, R. C.; Raetz, C. R.; Russell, D. W.; Subramaniam, S. Lmsd: Lipid Maps Structure Database. *Nucleic Acids Res.* **2007**, *35*, D527–D532.
- (7) Kaneda, T. Iso- and Anteiso-Fatty Acids in Bacteria: Biosynthesis, Function, and Taxonomic Significance. *Microbiol. Rev.* **1991**, *55*, 288–302.
- (8) Dufourc, E. J.; Smith, I. C. P.; Jarrell, H. C. The Role of Cyclopropane Moieties in the Lipid Properties of Biological Membranes: A Deuterium Nmr Structural and Dynamical Approach. *Biochemistry* **1984**, *23*, 2300–2309.
- (9) Raetz, C. R.; Whitfield, C. Lipopolysaccharide Endotoxins. *Annu. Rev. Biochem.* **2002**, *71*, 635–700.
- (10) Erridge, C.; Bennett-Guerrero, E.; Poxton, I. R. Structure and Function of Lipopolysaccharides. *Microbes Infect.* **2002**, *4*, 837–851.

- (11) De Rosa, M.; Gambacorta, A.; Gliozzi, A. Structure, Biosynthesis, and Physicochemical Properties of Archaeobacterial Lipids. *Microbiol. Rev.* **1986**, *50*, 70–80.
- (12) van Meer, G.; Voelker, D. R.; Feigenson, G. W. Membrane Lipids: Where They Are and How They Behave. *Nat. Rev. Mol. Cell Biol.* **2008**, *9*, 112–124.
- (13) Enkavi, G.; Javanainen, M.; Kulig, W.; Róg, T.; Vattulainen, I. Multiscale Simulations of Biological Membranes: The Challenge to Understand Biological Phenomena in a Living Substance. *Chem. Rev.* **2019**, *119*, 5607–5774.
- (14) Yang, Y.; Lee, M.; Fairn, G. D. Phospholipid Subcellular Localization and Dynamics. *J. Biol. Chem.* **2018**, *293*, 6230–6240.
- (15) Harayama, T.; Riezman, H. Understanding the Diversity of Membrane Lipid Composition. *Nat. Rev. Mol. Cell Biol.* **2018**, *19*, 281–296.
- (16) Murata, N.; Siegenthaler, P.-A. Lipids in Photosynthesis: An Overview. In *Lipids in Photosynthesis: Structure, Function and Genetics*; Paul-André, S.; Norio, M., Eds.; Springer: Netherlands: Dordrecht, 1998; pp 1–20.
- (17) Paradies, G.; Paradies, V.; Ruggiero, F. M.; Petrosillo, G. Role of Cardiolipin in Mitochondrial Function and Dynamics in Health and Disease: Molecular and Pharmacological Aspects. *Cells* **2019**, *8*, 643–650.
- (18) Gallala, H. D.; Sandhoff, K. Biological Function of the Cellular Lipid BMP-BMP as a Key Activator for Cholesterol Sorting and Membrane Digestion. *Neurochem. Res.* **2011**, *36*, 1594–1600.
- (19) Yoshida, S.; Uemura, M. Lipid Composition of Plasma Membranes and Tonoplasts Isolated from Etiolated Seedlings of Mung Bean (*Vigna Radiata* L.). *Plant Physiol.* **1986**, *82*, 807–812.
- (20) Maxfield, F. R.; van Meer, G. Cholesterol, the Central Lipid of Mammalian Cells. *Curr. Opin. Cell Biol.* **2010**, *22*, 422–429.
- (21) Boughter, C. T.; Monje-Galvan, V.; Im, W.; Klauda, J. B. Influence of Cholesterol on Phospholipid Bilayer Structure and Dynamics. *J. Phys. Chem. B* **2016**, *120*, 11761–11772.
- (22) Subczynski, W. K.; Pasenkiewicz-Gierula, M.; Widomska, J.; Mainali, L.; Raguz, M. High Cholesterol/Low Cholesterol: Effects in Biological Membranes Review. *Cell Biochem. Biophys.* **2017**, *75*, 369–385.
- (23) Zocher, F.; van der Spoel, D.; Pohl, P.; Hub, J. S. Local Partition Coefficients Govern Solute Permeability of Cholesterol-Containing Membranes. *Biophys. J.* **2013**, *105*, 2760–2770.
- (24) Gachumi, G.; El-Anead, A. Mass Spectrometric Approaches for the Analysis of Phytosterols in Biological Samples. *J. Agric. Food Chem.* **2017**, *65*, 10141–10156.
- (25) Weete, J. D.; Abril, M.; Blackwell, M. Phylogenetic Distribution of Fungal Sterols. *PLoS One* **2010**, *5*, No. e10899.
- (26) van den Brink-van der Laan, E.; Antoinette Killian, J.; de Kruijff, B. Nonbilayer Lipids Affect Peripheral and Integral Membrane Proteins Via Changes in the Lateral Pressure Profile. *Biochim. Biophys. Acta* **2004**, *1666*, 275–288.
- (27) Tonnesen, A.; Christensen, S. M.; Tkach, V.; Stamou, D. Geometrical Membrane Curvature as an Allosteric Regulator of Membrane Protein Structure and Function. *Biophys. J.* **2014**, *106*, 201–209.
- (28) Weigle, A. T.; Carr, M.; Shukla, D. Impact of Increased Membrane Realism on Conformational Sampling of Proteins. *J. Chem. Theory Comput.* **2021**, *17*, 5342–5357.
- (29) Venable, R. M.; Zhang, Y.; Hardy, B. J.; Pastor, R. W. Molecular Dynamics Simulations of a Lipid Bilayer and of Hexadecane: An Investigation of Membrane Fluidity. *Science* **1993**, *262*, 223–226.
- (30) Marrink, S. J.; Corradi, V.; Souza, P. C. T.; Ingólfsson, H. I.; Tieleman, D. P.; Sansom, M. S. P. Computational Modeling of Realistic Cell Membranes. *Chem. Rev.* **2019**, *119*, 6184–6226.
- (31) Klauda, J. B. Perspective: Computational Modeling of Accurate Cellular Membranes with Molecular Resolution. *J. Chem. Phys.* **2018**, *149*, No. 220901.
- (32) Jo, S.; Cheng, X.; Lee, J.; Kim, S.; Park, S.-J.; Patel, D. S.; Beaven, A. H.; Lee, K. I.; Rui, H.; Park, S.; Lee, H. S.; Roux, B.; MacKerell, A. D., Jr; Klauda, J. B.; Qi, Y.; Im, W. CHARMM-GUI Tool for Biomolecular Modeling and Simulation. *J. Comput. Chem.* **2017**, *38*, 1114–1124.
- (33) Jo, S.; Kim, T.; Im, W. Automated Builder and Database of Protein/Membrane Complexes for Molecular Dynamics Simulations. *PLoS One* **2007**, *2*, No. e880.
- (34) Venable, R. M.; Brown, F. L. H.; Pastor, R. W. Mechanical Properties of Lipid Bilayers from Molecular Dynamics Simulation. *Chem. Phys. Lipids* **2015**, *192*, 60–74.
- (35) Khakbaz, P.; Klauda, J. B. Probing the Importance of Lipid Diversity in Cell Membranes Via Molecular Simulation. *Chem. Phys. Lipids* **2015**, *192*, 12–22.
- (36) Park, S.; Beaven, A. H.; Klauda, J. B.; Im, W. How Tolerant Are Membrane Simulations with Mismatch in Area Per Lipid between Leaflets? *J. Chem. Theory Comput.* **2015**, *11*, 3466–3477.
- (37) Park, S.; Im, W.; Pastor, R. W. Developing Initial Conditions for Simulations of Asymmetric Membranes: A Practical Recommendation. *Biophys. J.* **2021**, *120*, 5041–5059.
- (38) Wu, E. L.; Engstrom, O.; Jo, S.; Stuhlsatz, D.; Yeom, M. S.; Klauda, J. B.; Widmalm, G.; Im, W. Molecular Dynamics and NMR Spectroscopy Studies of *E. coli* Lipopolysaccharide Structure and Dynamics. *Biophys. J.* **2013**, *105*, 1444–1455.
- (39) Wu, E. L.; Fleming, P. J.; Yeom, M. S.; Widmalm, G.; Klauda, J. B.; Fleming, K. G.; Im, W. *E. coli* Outer Membrane and Interactions with OmpLa. *Biophys. J.* **2014**, *106*, 2493–2502.
- (40) Kim, S.; Patel, D. S.; Park, S.; Slusky, J.; Klauda, J. B.; Widmalm, G.; Im, W. Bilayer Properties of Lipid A from Various Gram-Negative Bacteria. *Biophys. J.* **2016**, *111*, 1750–1760.
- (41) Luna, E.; Kim, S.; Gao, Y.; Widmalm, G.; Im, W. Influences of *Vibrio cholerae* Lipid A Types on LPS Bilayer Properties. *J. Phys. Chem. B* **2021**, *125*, 2105–2112.
- (42) Pandit, K. R.; Klauda, J. B. Membrane Models of *E. coli* Containing Cyclic Moieties in the Aliphatic Lipid Chain. *Biochim. Biophys. Acta* **2012**, *1818*, 1205–1210.
- (43) Im, W.; Khalid, S. Molecular Simulations of Gram-Negative Bacterial Membranes Come of Age. *Annu. Rev. Phys. Chem.* **2020**, *71*, 171–188.
- (44) Lim, J. B.; Klauda, J. B. Lipid Chain Branching at the Iso- and Anteiso-Positions in Complex *Chlamydia* Membranes: A Molecular Dynamics Study. *Biochim. Biophys. Acta* **2011**, *1808*, 323–331.
- (45) Pluhackova, K.; Horner, A. Native-Like Membrane Models of *E. coli* Polar Lipid Extract Shed Light on the Importance of Lipid Composition Complexity. *BMC Biol.* **2021**, *19*, No. 4.
- (46) Piggot, T. J.; Holdbrook, D. A.; Khalid, S. Electroporation of the *E. coli* and *S. aureus* Membranes: Molecular Dynamics Simulations of Complex Bacterial Membranes. *J. Phys. Chem. B* **2011**, *115*, 13381–13388.
- (47) Feng, S.; Wang, R.; Pastor, R. W.; Klauda, J. B.; Im, W. Location and Conformational Ensemble of Menaquinone and Menaquinol, and Protein-Lipid Modulations in Archaeal Membranes. *J. Phys. Chem. B* **2021**, *125*, 4714–4725.
- (48) Monje-Galvan, V.; Klauda, J. B. Modeling Yeast Organelle Membranes and How Lipid Diversity Influences Bilayer Properties. *Biochemistry* **2015**, *54*, 6852–6861.
- (49) Jo, S.; Lim, J. B.; Klauda, J. B.; Im, W. CHARMM-GUI Membrane Builder for Mixed Bilayers and Its Application to Yeast Membranes. *Biophys. J.* **2009**, *97*, 50–58.
- (50) Wu, E. L.; Qi, Y.; Song, K. C.; Klauda, J. B.; Im, W. Preferred Orientations of Phosphoinositides in Bilayers and Their Implications in Protein Recognition Mechanisms. *J. Phys. Chem. B* **2014**, *118*, 4315–4325.
- (51) Zhuang, X.; Ou, A.; Klauda, J. B. Simulations of Simple Linoleic Acid-Containing Lipid Membranes and Models for the Soybean Plasma Membranes. *J. Chem. Phys.* **2017**, *146*, No. 215103.
- (52) Ingólfsson, H. I.; Bhatia, H.; Zeppelin, T.; Bennett, W. F. D.; Carpenter, K. A.; Hsu, P.-C.; Dharuman, G.; Bremer, P.-T.; Schiödt, B.; Lightstone, F. C.; Carpenter, T. S. Capturing Biologically Complex Tissue-Specific Membranes at Different Levels of Compositional Complexity. *J. Phys. Chem. B* **2020**, *124*, 7819–7829.

- (53) van Eerden, F. J.; de Jong, D. H.; de Vries, A. H.; Wassenaar, T. A.; Marrink, S. J. Characterization of Thylakoid Lipid Membranes from Cyanobacteria and Higher Plants by Molecular Dynamics Simulations. *Biochim. Biophys. Acta* **2015**, *1848*, 1319–1330.
- (54) Ingólfsson, H. I.; Melo, M. N.; van Eerden, F. J.; Arnarez, C.; Lopez, C. A.; Wassenaar, T. A.; Periole, X.; de Vries, A. H.; Tieleman, D. P.; Marrink, S. J. Lipid Organization of the Plasma Membrane. *J. Am. Chem. Soc.* **2014**, *136*, 14554–14559.
- (55) Ingólfsson, H. I.; Carpenter, T. S.; Bhatia, H.; Bremer, P.-T.; Marrink, S. J.; Lightstone, F. C. Computational Lipidomics of the Neuronal Plasma Membrane. *Biophys. J.* **2017**, *113*, 2271–2280.
- (56) Zhuang, X.; Davila-Contreras, E. M.; Beaven, A. H.; Im, W.; Klauda, J. B. An Extensive Simulation Study of Lipid Bilayer Properties with Different Head Groups, Acyl Chain Lengths, and Chain Saturations. *Biochim. Biophys. Acta* **2016**, *1858*, 3093–3104.
- (57) Moradi, S.; Nowroozi, A.; Shahlaei, M. Shedding Light on the Structural Properties of Lipid Bilayers Using Molecular Dynamics Simulation: A Review Study. *RSC Adv.* **2019**, *9*, 4644–4658.
- (58) Lee, J.; Patel, D. S.; Stahle, J.; Park, S. J.; Kern, N. R.; Kim, S.; Lee, J.; Cheng, X.; Valvano, M. A.; Holst, O.; Knirel, Y. A.; Qi, Y.; Jo, S.; Klauda, J. B.; Widmalm, G.; Im, W. CHARMM-GUI Membrane Builder for Complex Biological Membrane Simulations with Glycolipids and Lipoglycans. *J. Chem. Theory Comput.* **2019**, *15*, 775–786.
- (59) Wu, E. L.; Cheng, X.; Jo, S.; Rui, H.; Song, K. C.; Davila-Contreras, E. M.; Qi, Y.; Lee, J.; Monje-Galvan, V.; Venable, R. M.; Klauda, J. B.; Im, W. CHARMM-GUI Membrane Builder toward Realistic Biological Membrane Simulations. *J. Comput. Chem.* **2014**, *35*, 1997–2004.
- (60) Keenan, T. W.; Morre, D. J. Phospholipid Class and Fatty Acid Composition of Golgi Apparatus Isolated from Rat Liver and Comparison with Other Cell Fractions. *Biochemistry* **1970**, *9*, 19–25.
- (61) Casares, D.; Escribá, P. V.; Rosselló, C. A. Membrane Lipid Composition: Effect on Membrane and Organelle Structure, Function and Compartmentalization and Therapeutic Avenues. *Int. J. Mol. Sci.* **2019**, *20*, No. 2167.
- (62) Henning, R.; Geidrich, H.-G. Membrane Lipids of Rat Liver Lysosomes Prepared by Freeflow Electrophoresis. *Biochim. Biophys. Acta* **1974**, *345*, 326–335.
- (63) Allan, D. Mapping the Lipid Distribution in the Membranes of BHK Cells (Mini-Review). *Mol. Membr. Biol.* **1996**, *13*, 81–84.
- (64) Horvath, S. E.; Daum, G. Lipids of Mitochondria. *Prog. Lipid Res.* **2013**, *52*, 590–614.
- (65) Olsson, J. M.; Eriksson, L. C.; Dallner, G. Lipid Compositions of Intracellular Membranes Isolated from Rat Liver Nodules in Wistar Rats. *Cancer Res.* **1991**, *51*, 3774–3780.
- (66) Tavernier, E.; LêQuôc, D.; LêQuôc, K. Lipid Composition of the Vacuolar Membrane of *Acet. Pseudoplatanus* Cultured Cells. *Biochim. Biophys. Acta* **1993**, *1167*, 242–247.
- (67) Kellermann, M. Y.; Yoshinaga, M. Y.; Valentine, R. C.; Wörmer, L.; Valentine, D. L. Important Roles for Membrane Lipids in Haloarchaeal Bioenergetics. *Biochim. Biophys. Acta* **2016**, *1858*, 2940–2956.
- (68) Bernat, P.; Paraszkiwicz, K.; Siewiera, P.; Moryl, M.; Płaza, G.; Chojniak, J. Lipid Composition in a Strain of *Bacillus subtilis*, a Producer of Iturin A Lipopeptides That Are Active against Uropathogenic Bacteria. *World J. Microbiol. Biotechnol.* **2016**, *32*, No. 157.
- (69) Eastman, P.; Swails, J.; Chodera, J. D.; McGibbon, R. T.; Zhao, Y.; Beauchamp, K. A.; Wang, L. P.; Simonnet, A. C.; Harrigan, M. P.; Stern, C. D.; Wiewiora, R. P.; Brooks, B. R.; Pande, V. S. OpenMM 7: Rapid Development of High Performance Algorithms for Molecular Dynamics. *PLoS Comput. Biol.* **2017**, *13*, No. e1005659.
- (70) Lee, J.; Cheng, X.; Swails, J. M.; Yeom, M. S.; Eastman, P. K.; Lemkul, J. A.; Wei, S.; Buckner, J.; Jeong, J. C.; Qi, Y.; Jo, S.; Pande, V. S.; Case, D. A.; Brooks, C. L., 3rd; MacKerell, A. D., Jr.; Klauda, J. B.; Im, W. CHARMM-GUI Input Generator for NAMD, GROMACS, AMBER, OpenMM, and CHARMM/OpenMM Simulations Using the CHARMM36 Additive Force Field. *J. Chem. Theory Comput.* **2016**, *12*, 405–413.
- (71) Hopkins, C. W.; Le Grand, S.; Walker, R. C.; Roitberg, A. E. Long-Time-Step Molecular Dynamics through Hydrogen Mass Repartitioning. *J. Chem. Theory Comput.* **2015**, *11*, 1864–1874.
- (72) Gao, Y.; Lee, J.; Smith, I. P. S.; Lee, H.; Kim, S.; Qi, Y.; Klauda, J. B.; Widmalm, G.; Khalid, S.; Im, W. CHARMM-GUI Supports Hydrogen Mass Repartitioning and Different Protonation States of Phosphates in Lipopolysaccharides. *J. Chem. Inf. Model.* **2021**, *61*, 831–839.
- (73) Ryckaert, J.-P.; Ciccotti, G.; Berendsen, H. J. C. Numerical Integration of the Cartesian Equations of Motion of a System with Constraints: Molecular Dynamics of N-Alkanes. *J. Comput. Phys.* **1977**, *23*, 327–341.
- (74) Steinbach, P. J.; Brooks, B. R. New Spherical-Cutoff Methods for Long-Range Forces in Macromolecular Simulation. *J. Comput. Chem.* **1994**, *15*, 667–683.
- (75) Essmann, U.; Perera, L.; Berkowitz, M. L.; Darden, T.; Lee, H.; Pedersen, L. G. A Smooth Particle Mesh Ewald Method. *J. Chem. Phys.* **1995**, *103*, 8577–8593.
- (76) Åqvist, J.; Wennerström, P.; Nervall, M.; Bjelic, S.; Brandsdal, B. O. Molecular Dynamics Simulations of Water and Biomolecules with a Monte Carlo Constant Pressure Algorithm. *Chem. Phys. Lett.* **2004**, *384*, 288–294.
- (77) Chow, K.-H.; Ferguson, D. M. Isothermal-Isobaric Molecular Dynamics Simulations with Monte Carlo Volume Sampling. *Comput. Phys. Commun.* **1995**, *91*, 283–289.
- (78) Pogozheva, I. D.; Tristram-Nagle, S.; Mosberg, H. I.; Lomize, A. L. Structural Adaptations of Proteins to Different Biological Membranes. *Biochim. Biophys. Acta* **2013**, *1828*, 2592–2608.
- (79) Hechtberger, P.; Zinser, E.; Saf, R.; Hummel, K.; Paltauf, F.; Daum, G. Characterization, Quantification and Subcellular Localization of Inositol-Containing Sphingolipids of the Yeast, *Saccharomyces cerevisiae*. *Eur. J. Biochem.* **1994**, *225*, 641–649.
- (80) Daleke, D. L. Regulation of Transbilayer Plasma Membrane Phospholipid Asymmetry. *J. Lipid Res.* **2003**, *44*, 233–242.
- (81) Kučerka, N.; Nagle, J. F.; Sachs, J. N.; Feller, S. E.; Penczer, J.; Jackson, A.; Katsaras, J. Lipid Bilayer Structure Determined by the Simultaneous Analysis of Neutron and X-Ray Scattering Data. *Biophys. J.* **2008**, *95*, 2356–2367.
- (82) Kim, S.; Chang, R. Structure, Dynamics, and Phase Behavior of DOPC/DSPC Mixture Membrane Systems: Molecular Dynamics Simulation Studies. *Bull. Korean Chem. Soc.* **2016**, *37*, 1076–1085.
- (83) Rawicz, W.; Olbrich, K. C.; McIntosh, T.; Needham, D.; Evans, E. Effect of Chain Length and Unsaturation on Elasticity of Lipid Bilayers. *Biophys. J.* **2000**, *79*, 328–339.
- (84) Kučerka, N.; Tristram-Nagle, S.; Nagle, J. F. Structure of Fully Hydrated Fluid Phase Lipid Bilayers with Monounsaturated Chains. *J. Membr. Biol.* **2006**, *208*, 193–202.
- (85) Benning, C. Mechanisms of Lipid Transport Involved in Organelle Biogenesis in Plant Cells. *Annu. Rev. Cell Dev. Biol.* **2009**, *25*, 71–91.
- (86) Schoepp-Cothenet, B.; Lieutaud, C.; Baymann, F.; Verméglio, A.; Friedrich, T.; Kramer, D. M.; Nitschke, W. Menaquinone as Pool Quinone in a Purple Bacterium. *Proc. Natl. Acad. Sci. U.S.A.* **2009**, *106*, 8549–8554.
- (87) Velikova, V.; Edreva, A.; Loreto, F. Endogenous Isoprene Protects Phragmites Australis Leaves against Singlet Oxygen. *Physiol. Plant.* **2004**, *122*, 219–225.
- (88) Nikaido, H. Molecular Basis of Bacterial Outer Membrane Permeability Revisited. *Microbiol. Mol. Biol. Rev.* **2003**, *67*, 593–656.
- (89) Nikaido, H. Outer Membranes, Gram-Negative Bacteria. In *Encyclopedia of Microbiology*, 3rd ed.; Schaechter, M., Ed.; Academic Press: Oxford, U.K., 2009; Vol. 52, pp 439–452.
- (90) Snyder, S.; Kim, D.; McIntosh, T. J. Lipopolysaccharide Bilayer Structure: Effect of Chemotype, Core Mutations, Divalent Cations, and Temperature. *Biochemistry* **1999**, *38*, 10758–10767.
- (91) Koga, Y. Thermal Adaptation of the Archaeal and Bacterial Lipid Membranes. *Archaea* **2012**, *2012*, No. 769652.

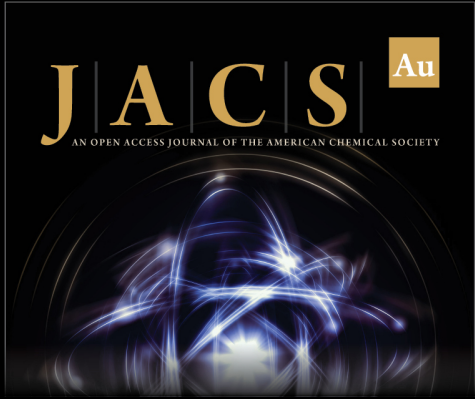
(92) Mansilla, M. C.; de Mendoza, D. The *Bacillus subtilis* Desaturase: A Model to Understand Phospholipid Modification and Temperature Sensing. *Arch. Microbiol.* **2005**, *183*, 229–235.

(93) Gallová, J.; Uhríková, D.; Kučerka, N.; Teixeira, J.; Balgavý, P. Hydrophobic Thickness, Lipid Surface Area and Polar Region Hydration in Monounsaturated Diacylphosphatidylcholine Bilayers: Sans Study of Effects of Cholesterol and β -Sitosterol in Unilamellar Vesicles. *Biochim. Biophys. Acta* **2008**, *1778*, 2627–2632.

(94) Rawicz, W.; Smith, B. A.; McIntosh, T. J.; Simon, S. A.; Evans, E. Elasticity, Strength, and Water Permeability of Bilayers That Contain Raft Microdomain-Forming Lipids. *Biophys. J.* **2008**, *94*, 4725–4736.

(95) Marsh, D. Membrane Water-Penetration Profiles from Spin Labels. *Eur. Biophys. J.* **2002**, *31*, 559–562.

(96) Jo, S.; Kim, T.; Iyer, V. G.; Im, W. Charmm-Gui: A Web-Based Graphical User Interface for CHARMM. *J. Comput. Chem.* **2008**, *29*, 1859–1865.



JACS Au
AN OPEN ACCESS JOURNAL OF THE AMERICAN CHEMICAL SOCIETY

Editor-in-Chief
Prof. Christopher W. Jones
Georgia Institute of Technology, USA

Open for Submissions 

pubs.acs.org/jacsau  ACS Publications
Most Trusted. Most Cited. Most Read.